

Lawrence Berkeley National Laboratory

Recent Work

Title

ALMOST EVERYTHING ABOUT BARYON RESONANCES

Permalink

<https://escholarship.org/uc/item/5952x3hk>

Author

Rosenfeld, Arthur H.

Publication Date

1973-07-01

Lectures presented at the School of
Subnuclear Physics, Erice, Italy,
July 10-24, 1973.

LBL-2098

c.1

ALMOST EVERYTHING ABOUT BARYON RESONANCES

Arthur H. Rosenfeld

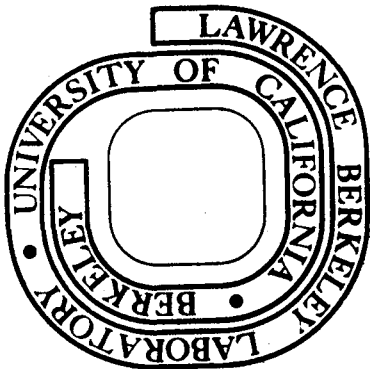
DEC 9 1974

July 1973

Prepared for the U. S. Atomic Energy Commission
under Contract W-7405-ENG-48

For Reference

Not to be taken from this room



LBL-2098

c.1

DISCLAIMER

This document was prepared as an account of work sponsored by the United States Government. While this document is believed to contain correct information, neither the United States Government nor any agency thereof, nor the Regents of the University of California, nor any of their employees, makes any warranty, express or implied, or assumes any legal responsibility for the accuracy, completeness, or usefulness of any information, apparatus, product, or process disclosed, or represents that its use would not infringe privately owned rights. Reference herein to any specific commercial product, process, or service by its trade name, trademark, manufacturer, or otherwise, does not necessarily constitute or imply its endorsement, recommendation, or favoring by the United States Government or any agency thereof, or the Regents of the University of California. The views and opinions of authors expressed herein do not necessarily state or reflect those of the United States Government or any agency thereof or the Regents of the University of California.

Lectures at the School of Subnuclear Physics, Erice July 10-24, 1973

ALMOST EVERYTHING ABOUT BARYON RESONANCES

Arthur H. Rosenfeld

Department of Physics and Lawrence Berkeley Laboratory

University of California, Berkeley, California 94720

Contents

LECTURE I :- FROM EVENTS TO ARGAND DIAGRAMS

1. Introduction, Recent Doubling of Information.
2. Partial-Wave Analysis of $\pi N \rightarrow N\pi\pi$.
3. Connection a) Between Energies and b) to Elastic Partial Waves.
4. Counting and Naming the Waves.
5. Checks of the LBL/SLAC Programs.
6. Results: Argand Diagrams (1972 Solution Only).

LECTURE II :- FROM ARGAND DIAGRAMS TO PHYSICS

1. Comparisons: $\pi N \rightarrow \rho N$ and $\gamma p \rightarrow \pi N$ with the Quark Model.
2. SU(3) Tests: $\pi N \rightarrow \Delta\pi$ and $KN \rightarrow \Sigma(1385)\pi$.
3. Comparison of $\Delta\pi$ amplitudes with SU(6) and Quark Model.
4. Estimating Resonance Parameters "by eye", without a K-matrix.
5. Multichannel K-matrix fits.
6. Breit-Wigner "Refit" to K-matrix fits.
7. Comparison of Different Resonance Parametrizations.
8. Conclusions.

LECTURE I.

1. INTRODUCTION. RECENT DOUBLING OF INFORMATION

The title for these talks is both too ostentatious and too short, but in one line I could not add that I shall confine myself to Non-Strange Baryon Resonances which I'll call N^* s. I'll show that the interesting information on most of these states has roughly doubled in the last year or so, permitting some interesting tests of $SU(6)$ and the Quark Model.

Until roughly last year, almost all quantitative information on N^* resonances came from Elastic Partial - Wave Analyses ($\pi N \rightarrow \pi N$), which are still called "Elastic Phase Shift Analyses" or "EPSA" for short. Two excellent recent examples are the work of Almeded and Lovelace (CERN-72)¹⁾ and of Ayed, Bareyre and Lemoigne (Saclay 72)²⁾. Some of the photon couplings had been measured in photo-production experiments ($\gamma N \rightarrow \pi N$)³⁾, and one could not find any Argand Diagrams for $N^* \rightarrow \Delta\pi, N\rho$, etc.

But suddenly there are several computer programs capable of doing a partial-wave analysis of

$$\pi N \rightarrow I(J^P) \rightarrow N\pi\pi \quad (1)$$

in terms of the "Isobar Model", i.e.

$$N\pi\pi = \Delta\pi + N\rho + N\epsilon + \dots \quad (2)$$

At first it seems scandalous that such information comes so late, but remember the situation in "EPSA". Resonances were not disentangled until good polarization data became available about 10 years ago. The equivalent to polarization in $N\pi\pi$ analyses is the interference between the various resonance bands on an $N\pi\pi$ Dalitz plot. So one has to analyse the whole Dalitz plot, using about 10,000 events at a single energy. That takes big programs, both experimental and computational.

To convince you that the available information has really doubled recently, I present Table 1. Actually, more interesting than the new partial widths for $\Delta\pi, N\rho, \dots$, is the fact that the sign of the amplitude is now known for each channel. And we'll be able to compare the imaginary part of the newly-found pole position with the new partial widths.

So when I say that we now know "almost everything" about N^* s I mean that the only obvious reaction that has not been measured and analysed is $\pi N \rightarrow N\pi\pi$ with a polarized target. That would be the most efficient way to find the couplings, but in fact, if the forth-coming unpolarized analyses are really unique, the problem may be solved before the polarization experiments are done.

2. PARTIAL WAVE ANALYSIS OF $\pi N \rightarrow N\pi\pi$

A total of five charge channels can be fitted :-

$$\pi^- p \rightarrow n\pi^- \pi^+, \quad p\pi^- \pi^0, \quad n\pi^0 \pi^0, \quad (3)$$

$$\pi^+ p \rightarrow p\pi^+ \pi^0, \quad n\pi^+ \pi^+. \quad (4)$$

At $E_{c.m.} = 1520 \text{ MeV} \sim 13 \text{ mb}$ of the total inelastic $\pi^- p$ cross section of 15 mb is accounted for by reactions (3) while at $E_{c.m.} = 1700 \text{ MeV}$ the numbers are respectively 21-22 mb out of $\sim 25 \text{ mb}$. Reaction (4) is also large.

Thus to restate more quantitatively my introductory comment, we conclude that if the $N\pi\pi$ final states can be understood we will have an essentially complete description of πN scattering at these energies. We will then be in a position to attempt a multichannel analysis of the πN reactions with the added knowledge that no further new experimental information will become available (although, of course, the present inelastic partial wave amplitudes may be somewhat modified in light of new results; e.g., polarization measurements in the inelastic reactions).

In general two methods have been followed : isobar model analyses of the whole final state^{5,6)}, and straight, quasi-two-body partial-wave analysis of specific reactions, e.g., $\pi N \rightarrow \Delta\pi$ (Ref. 7) which have been isolated by applying judicious cuts to the data to select this final state.

2.1. Isobar model

Groups at Oxford^{8,9)}, Saclay¹⁰⁾ and LBL/SLAC¹¹⁾ have used this technique, differing mainly in their methods of fitting the data. The method itself consists of writing the transition amplitude for reaching a given $N\pi\pi$ final state as a coherent sum of quasi-two-body processes as indicated in Fig. 1. The transition matrix is then written in an LS representation as^{5,6)}

$$T(W, w_1, w_2, \theta, \phi) = \sum_{IJLL'S\ell} A^{IJLL'S\ell} \times C^{I_X JLL'S\ell} (w_1, w_2, \theta, \phi) F^\ell(w_1, w_2), \quad (5)$$

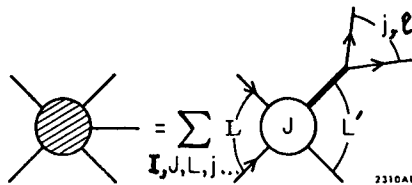


FIG. 1--The isobar model.

Table 1. Recent doubling of information available on a typical resonance: F_{35}

a. Entry in 1972 Particle Data Booklet.

b. Extra information in 1973 edition, or to appear in 1974

State	$I(J^P)$	Mass (MeV)	Width (MeV)	<u>Partial Widths</u>	
				Mode	(MeV)
<u>a. 1972 Entries</u>					
$\Delta(1890)$	$3/2(5/2^+)$	F_{35}	1840 to 1920	135 to 350	$N\pi$ $N\pi\pi$ 50 large
<u>b. 1973 or 1974 Additions</u>					
Pole at 1824 - i $\frac{282}{2}$				$N_{\pi\pi}$ {	[$\Delta\pi$ 55] [$N\rho$ 219]
Breit-Wigner "Refit" :-		1907	324	$N\gamma$.03
				Sum	324

where : $W, w_1, w_2, \theta, \phi$ are the kinematic variables required to completely specify the reaction; C^I is the product of isospin Clebsch-Gordon coefficients to reach different charge final states; $X^{JLL'S\ell}$ contains all factors related to the angular momentum decompositions, including barrier factors; $F^\ell(w_1, w_2)$ is the Final State enhancement factor e.g., a Breit-Wigner or Watson final state interaction factor,¹²⁾ where ℓ is the orbital angular momentum in the decay of the isobar. The variable parameters, the partial wave amplitudes, $A^{IJLL'S\ell}$ are assumed to be dependent only on the total c.m. energy W . The differential cross section is

$$d^4\sigma(W, w_1, w_2, \theta, \phi) \propto |T(W, w_1, w_2, \theta, \phi)|^2 \quad (6)$$

The data are fitted in a variety of manners by the different groups, always treating each c.m. energy independently - Oxford^{8,9)} fit invariant mass and angular projections of the data in π^+p collisions for $1300 < E < 1500$; Saclay¹⁰⁾ fit moments of the angular distribution for several zones on the Dalitz plot. The old analysis covered π^-p and π^+p separately: π^-p ($1390 < E < 1580$) and π^+p ($1650 < E < 1970$); the new analysis uses π^+p and π^-p , starting at 1390 MeV ; LBL/SLAC¹¹⁾ make maximum likelihood fits to π^+p reactions for $1300 < E < 1970$ (ie., to all the kinematic variables).

This isobar-model approach is optimistic in that one hopes to fit the whole reaction, making maximum use of all interference effects associated with the overlap of the various resonance bands. However, as we shall see this has proved to be possible (for at least 10,000 events at each energy) and provides us with an immense amount of information.

2.2. Single-Channel Partial-Wave analyses (e.g. $\pi N \rightarrow \Delta \pi$).

The LBL/SLAC¹³⁾ collaboration, and an LBL/UC Riverside¹⁴⁾ group, have used this technique to analyse specifically

$$\pi N \rightarrow \pi \Delta \quad (7)$$

After applying cuts, one assumes that one has a pure sample of reactions (7) and then performs fits to the production angular distribution of the Δ and sometimes also its density matrix elements, in terms of the partial wave amplitudes, usually with an energy dependent formalism. [These single-channel analyses throw away so much interference information that it is no longer possible to get unique fits at a single energy.] The major advantage of the single-channel analysis is that the formalism is easier to handle, whereas the great dangers lie in the assumption of a pure sample and in the energy-dependent parametrizations one uses. Furthermore, it is impossible to relate in phase, reactions such as

$$\pi N \rightarrow N \rho \quad (8)$$

to reaction (7) because the regions of interference which would define the phase are specifically removed from consideration. I feel that this method provides useful information but only on the large unambiguous partial waves present, and one should be much more skeptical of small effects¹³⁾.

2.3. Justification of the Isoobar Model.

We think that the Isoobar Model is a theoretically adequate way to analyse the data, and Smadja¹⁵⁾ estimates that the approximations involved affect our amplitudes by $< 5\%$, i.e. $\delta T < .025$: This is tiny compared to our stated accuracy of $\delta T \approx 0.1$ (see sect. 5.2), or even our statistical error $\delta T(\text{stat.}) \approx 0.03$ at a single energy. Nevertheless the theoretical approximations are interesting, so I'll outline them.

a) Even if only one final-state resonance were involved, we don't know precisely how to write the final state enhancement factor. We all use Watson's¹²⁾ $e^{i\delta} \sin \delta$ because it's simple and consistent with observation, but it is not unique¹⁶⁾ and it could be more complicated.

b) Consider our case, when resonances overlap. For example, consider $\pi^- p \rightarrow S_{11} \rightarrow \Delta^- \pi^+(L'=0) + n \rho^0(L'=0)$. For the first term by definition we include the factor $e^{i\delta} \sin \delta$ for the N and π composing the Δ . For the second ($N\rho$) term we do not provide for any Δ . But of course there is some probability that the n and the π^- from the ρ will be in an $I = \frac{3}{2}$ p-wave. This is what can introduce the 5% error in our results. The error is proportional to the overlap $\langle \Delta \pi | N \rho \rangle$ between $\Delta \pi$ and $N \rho$ wave functions which in any case we have to calculate to compute the cross section, Eqs. (5) and (6).

2.4. Isobar Model Analyses of 3π and $K2\pi$ Production.

The Illinois groups of Ascoli and Kruse have pioneered the isobar analysis of the 3π subsystem produced in the reaction $\pi p \rightarrow p3\pi$, according to the model

$$3\pi \rightarrow I(J^P) \rightarrow \rho\pi + \epsilon\pi. \quad (9)$$

Here $I(J^P) = 1(1^+)$ corresponds to the partial wave associated with the A_1 meson, $1(2^+)$ corresponds to the A_2 , etc. I need not discuss the interesting results; you can read David Miller's contribution to these same proceedings. But I can mention that Ed Ronat at LBL is fitting 7 GeV $\pi^+p \rightarrow p(3\pi)^+$ events with the LBL/SLAC¹¹⁾ programs and seems qualitatively to be confirming the results obtained with the Ascoli program, which uses a rather different parametrization. It is hard to write and debug these complicated programs (see Sect. 5), so this confirmation should be a relief to all concerned. The $N\pi\pi$ fits of Eq. (2) require up to 60 isobar-model waves, and so need $\geq 10,000$ events at each energy; the 3π fits of Eq. (9) need only a dozen waves, and Ascoli and Kruse achieved their first fits with only $\sim 15,000$ events spread over half a dozen energies.

In addition to 3π systems, isobar-model programs are now being used on $K\pi\pi$ (the problem of the Q^- "meson") and on $NK\pi$ (the question of a Z_1^* "resonance").¹⁷⁾

3. CONNECTION a) BETWEEN ENERGIES AND b) TO ELASTIC PARTIAL WAVES

Before we proceed, we should define some notation. Because there are pion beams, and no ρ or Δ beams, we call the πN channel "number 1", and the reaction $\pi N \rightarrow \pi N$ we call "elastic". For each incoming partial wave, $I(J^P)$, we define the T-matrix by

$$\left. \begin{array}{l} \sigma(\pi N \rightarrow N\pi) \\ \sigma(\pi N \rightarrow N\pi\pi) \\ \sigma(\pi N \rightarrow N\gamma) \end{array} \right\} = 4\pi\lambda^2(J+\frac{1}{2}) \left\{ \begin{array}{l} |T_{11}|^2 \\ |T_{1\Delta} + T_{1\rho} + T_{1\epsilon} + \dots|^2 \\ |T_{1\gamma}|^2 \end{array} \right\} \quad (10)$$

The values of the magnitude and phase of $T_{11}(I, J^P, E_1)$ are already known from "EPSA", and we want to take advantage of this valuable and expensive information.

After a single-energy $N\pi\pi$ fit we know the magnitude and relative phase of the inelastic terms $T_{1\Delta}$, $T_{1\rho}$, ... but one crucial overall phase is still free, and must be tied to that of T_{11} .

In addition, before we present an Argand Diagram, we want to impose two constraints :

1. Continuity in Energy.
2. Unitarity simultaneously on all the elements of the T-matrix. Specifi-

cally the S-matrix, $S = 1 + 2iT$, must be unitary and symmetric.

We can tie the overall inelastic phase to the EPSA phase, and impose these two constraints by means of an energy-dependent, multi-channel K-matrix fit simultaneously to the T_{11} amplitudes from EPSA and the off-diagonal T_{1j} from our own fits. More details are given in Sect. 4 of Lecture II - here I want merely to outline the battle plan. For the moment let me just say that if we write the matrix equation for each J^P

$$S = \frac{1+iK}{1-iK} = 1 + 2iT, \quad (11)$$

then if K is real and symmetric, S will be unitary and symmetric (i.e. will satisfy unitarity, and time-reversal invariance). Solving (11) for the T-matrix for each J^P we have

$$T = \frac{K}{1-iK}, \quad (12)$$

so we can parametrize T in terms of a real, symmetric matrix. Moreover we shall write K as a sum of factorizable poles (corresponding to a sum of resonances in T) plus a non-factorizable background (linear in c.m. energy E) :

$$K_{ij} = \sum_{R=1}^3 \frac{\gamma_i \gamma_j}{E_R - E} + B_{ij} + C_{ij} E. \quad (13)$$

For each J^P we then get K-matrix parameters from our fit to all available amplitudes (typically three, but for D_{13} we need five) at 20 different energies.

From the K-matrix parameters we can extract smooth Argand diagrams. This procedure is summarized in Fig. 2. [As you can see, we go on even further, but that is reserved for Lecture II, Sect. 6]. You should now have enough of an outline to understand the Argand plots at the end of this section.

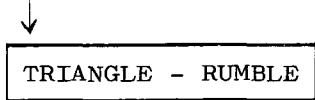
The final reaction, $\pi N \rightarrow N\gamma$ (inverse photoproduction) has such a small cross section ($\propto \omega^2$) that unitarity is no help, and we do not include it in the K-matrix fit. Instead the K-matrix parameters from the hadronic reactions are used as starting values for a final energy-dependent K-matrix fit to photoproduction. This is discussed in Lecture II, Sect. 1.

4. COUNTING AND NAMING THE WAVES

How many isobar model waves can be fed by a single incoming πN partial wave, e.g. D_{13} ? If you peek ahead at Fig. 9, you will see that the answer is at least 5.

- a. D_{13} can feed two $\Delta\pi$ waves, i.e. the Δ can be produced in a D-wave ($L = L' = 2$ in the notation of Fig. 1), or even more likely in an S-wave ($L' = 0$, $j_{\Delta} = \frac{3}{2}$, $\underline{L}' + \underline{j}_{\Delta} = \underline{J} = \frac{3}{2}$). We call these waves ΔDD_{13} and ΔDS_{13}

Input :- 10,000 $N\pi\pi$ events at one energy E_i .

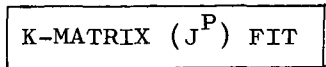


↓

Output :- { About 24 partial wave amplitudes $T_\alpha(E_i)$, i.e one energy }
 { point ready for 24 different Argand plots. }

Sorting :- From now on each incoming partial wave is treated separately.

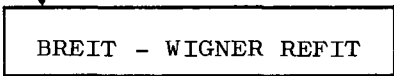
Input : { Amplitudes $T_{l\alpha}$ for 20 different energies, several channels, e.g. }
 { Channel 1 :- $\pi N \rightarrow F_{15} \rightarrow N\pi$ from CERN or Saclay. }
 { 2 :- $\rightarrow \Delta\pi$ }
 { 3 :- $\rightarrow N\rho$ } from Triangle - Rumble
 { 4 :- etc., see Figs 7 - 13. }



↓

Output :→ { K-matrix parameters and smooth Argand Plots $T_{\alpha\beta}^{J^P}(E)$ }

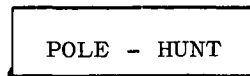
Input :←



↓

Output: B.W. Parameters near E_R for

$$T_{\alpha\beta} = \frac{\frac{1}{2} \sqrt{\Gamma_\alpha \Gamma_\beta}}{E_R - E - i\Gamma/2} + B_{\alpha\beta} + C_{\alpha\beta} E.$$



↓

Output : Pole Position

$$m_{\text{Real}} - i \frac{\Gamma}{2}$$

Compare direct values with those obtained indirectly from BW Refit.

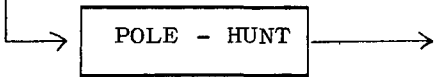


Fig. 2. Sequence of extracting Argand Plots and parameters for Resonances.

and in fact find some of both amplitudes.

- b. D_{13} can in principle feed three ρN waves. The spin of the ρ ($j = 1$ in fig. 1) can couple with the spin of the nucleon to form $S = \frac{1}{2}$ or $\frac{3}{2}$. If $S = \frac{1}{2}$, L' can take only one value, and we call the wave $\rho_1 DD_{13}$. If $S = \frac{3}{2}$, L' can be a D- or an S-wave, and we write $\rho_3 DD_{13}$ and $\rho_3 DS_{13}$. In Fig. 9 we report evidence for only the last of these three waves.
- c. We give the name " ϵ " to an s-wave dipion [$I(J^P) = 0(0^+)$]. Then an incoming $\pi N D_{13}$ wave can feed only ϵDP_{13} .

So, if we include the πN channel, D_{13} could be coupled to 7 decay channels, and we find we need 5 of them (but 2,3 is more typical).

If we confine our analysis to F waves or less ($L \leq 3$, $L' \leq 3$) we find that 14 incoming waves (7 with $I = \frac{1}{2}$ - S_{11} through F_{17} - plus 7 with $I = \frac{3}{2}$) can in principle feed 60 inelastic waves. Our program searches for all 60 complex amplitudes (119 real numbers) but we find a need for only about half of them, and in fact in the region at or below 1520 MeV, only for a quarter of them.

5. CHECKS OF THE LBL/SLAC PROGRAMS

5.1 The LBL/SLAC Analysis

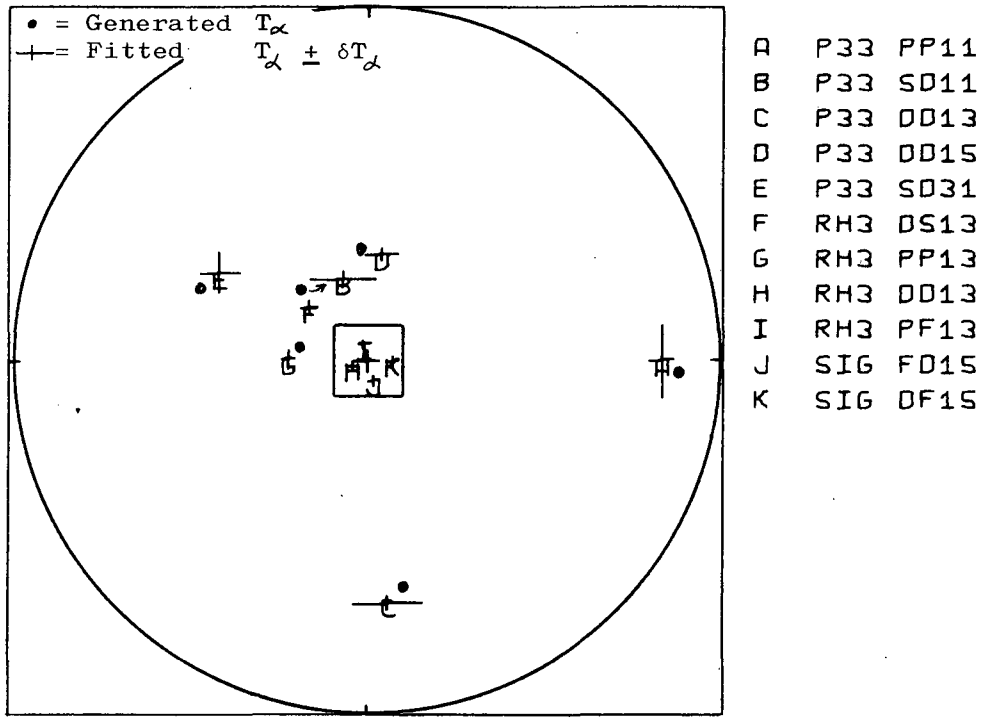
For the rest of this Lecture I shall concentrate on the LBL/SLAC $N\pi\pi$ analysis, which is the only one which has presented Argand plots of all channels at 18 energies from 1300 to 2000 MeV. It is well documented. The most recent publication is by Cashmore¹⁸⁾, in the Proceedings of the 1973 Purdue Conference. See also Refs. 6 and 11.

This analysis has the following advantages :

- i) It spans the c.m. energy range $1300 < E < 2000$ except for a 100 MeV gap $1540 < E < 1650$, where the data are still being analysed by Saclay.
- ii) It utilizes the data in the most efficient manner, making a simultaneous max. likelihood fit^{11,19)} to the three major channels at each energy

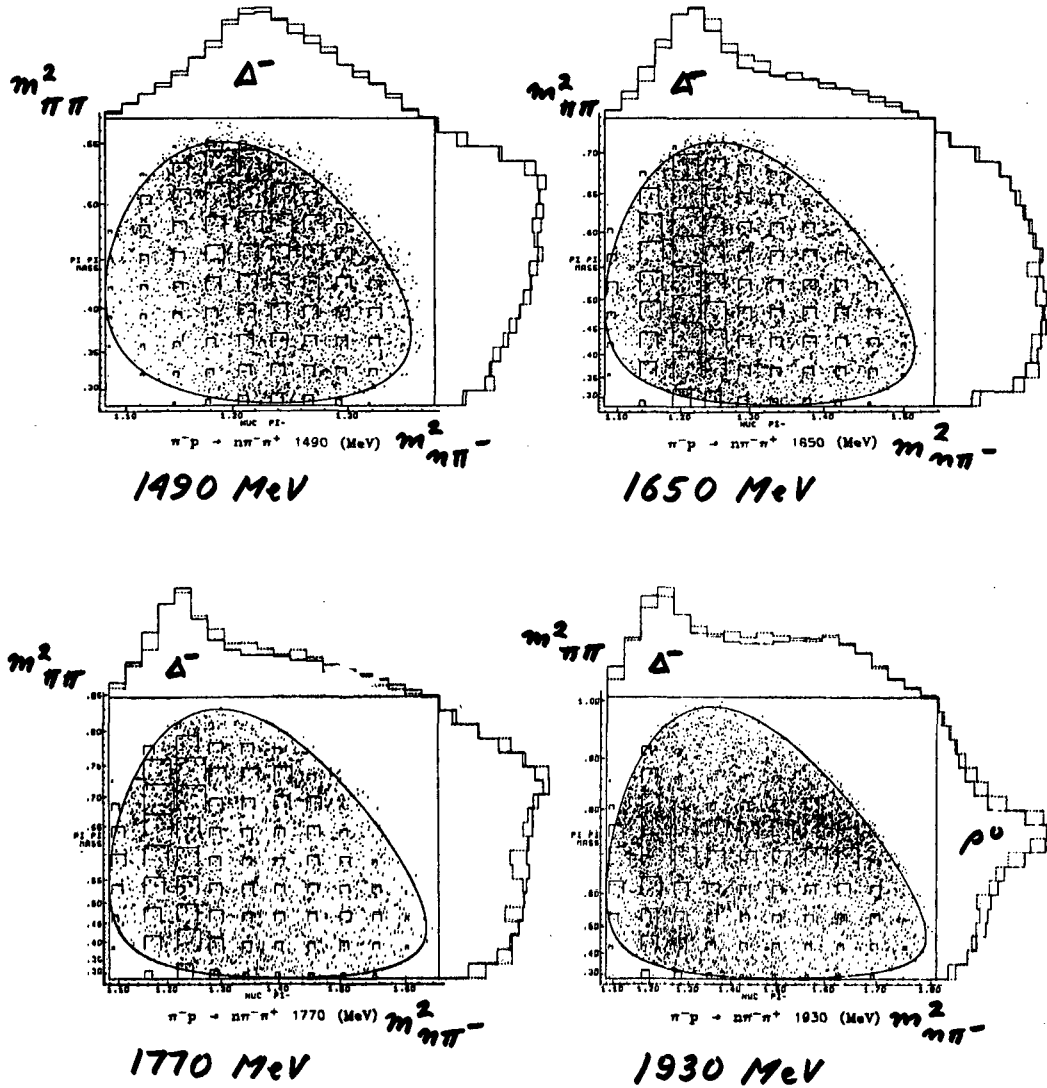
$$\begin{aligned} \pi^- p &\rightarrow n\pi^-\pi^+ \\ \pi^- p &\rightarrow p\pi^-\pi^0 \\ \pi^+ p &\rightarrow p\pi^+\pi^0 \end{aligned} \tag{14}$$

- iii) We obtain excellent agreement with the inelastic reaction cross sections predicted by elastic phase shift analyses (EPSA). (We used 1970 solutions, by now, unfortunately, obsolete).
- iv) From the single-energy fits at each energy we have been able to establish two continuous solutions over the full energy range, thus producing



XBL 726-934

Fig. 3 - Results of a fit to 7500 Monte Carlo events generated at 1650 MeV to test Triangle/Rumble. This is Figure 8 of Herndon's thesis²⁰⁾.



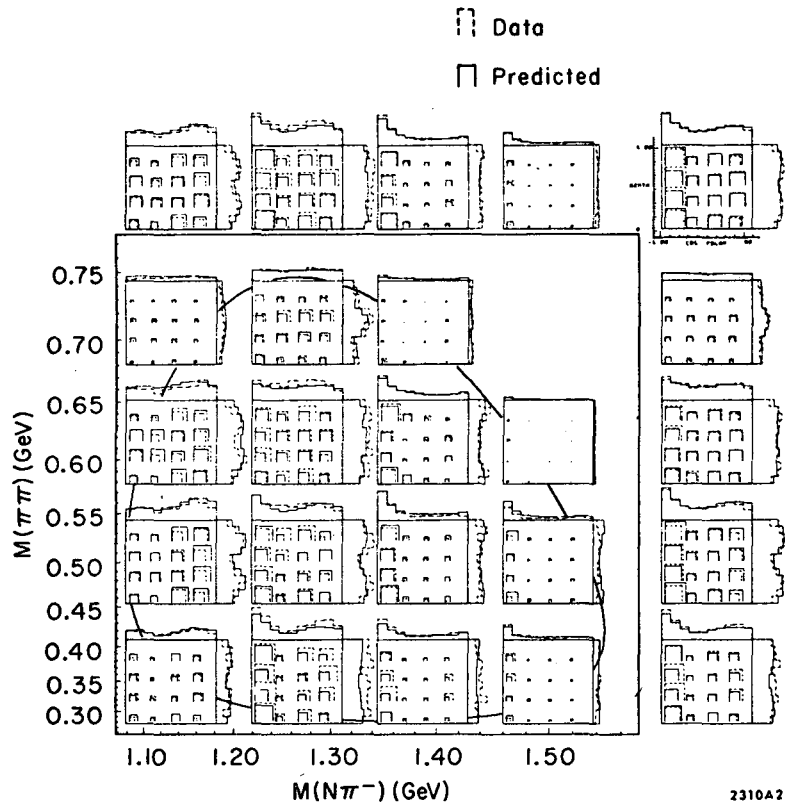
XBL 727-1289

Fig. 4 - Dalitz plot for $\approx 5000 \pi^- p \rightarrow nn^- \pi^+$ events at four specimen energies. Each projection shows two histograms :- dashed lines represent data, solid lines are predictions from the fit. This is Fig. 1.1 of Ref. 11.

TABLE 2

Summary of χ^2 at specimen energies. The predicted bin populations are derived from maximum likelihood fits to the data.

$E_{c.m.}$	χ^2	N_{bins}	Number of Partial Waves
1530	790	681	15
1690	1086	679	20
1970	2372	702	24



2310A2

FIG. 5 -Fits to the reaction $\pi^- p \rightarrow \pi^+ \pi^- n$ at a c.m. energy of 1690 MeV. The figure contains $\cos \theta$ vs ϕ plots for individual regions of the Dalitz plot where $\cos \theta$ and ϕ are the polar angles of the incident pion in a coordinate system defined by the final state. The z axis lies along \vec{p}_N and the y axis lies along $\vec{p}_\pi^- \times \vec{p}_{\pi^+}$. The plots outside the Dalitz plot are the sums of the corresponding plots within the boundary.

5.4 Adequacy of fits

The satisfactory quality of our fits is illustrated by Table 2 and by Figs. 4, 5, and 6. Table 2 represents the χ^2 at 3 energies in our analysis, the ratio χ^2/N being excellent at lower energies but deteriorating as the energy increases. There are enormous variations of structure within the data at a given energy and in general the model reproduces them well, as can be seen in Fig. 4 (a standard Dalitz plot) and in Fig. 5, which shows our 4-D representation of the fit to $\pi^+\pi^-\pi^0$ at 1690 MeV.

Figure 5 consists of 2-D plots of the angular variables, $\cos \Theta$ and ϕ for individual regions of the Dalitz plot. We can also use our partial wave amplitudes to predict the cross section for

$$\pi^-p \rightarrow n\pi^0\pi^0 \quad (15)$$

and the good agreement with the experimental results is demonstrated in Fig. 6a. Finally, and this will be continually apparent throughout this talk, we have excellent agreement with the 1970 EPSA predictions.

The remaining point that must be addressed is the question of uniqueness of the solutions. For energies below 1540 MeV we are fairly certain of a unique solution because many random starting values always lead to one final solution. For energies greater than 1650 MeV we cannot be certain. We obtain several solutions at each energy from which we have identified the present solutions by requiring reasonable agreement with EPSA predictions and continuity of the solution at the adjacent energy point. This continuity, in modulus and phase, is vitally important because it allows us to show Argand diagrams.

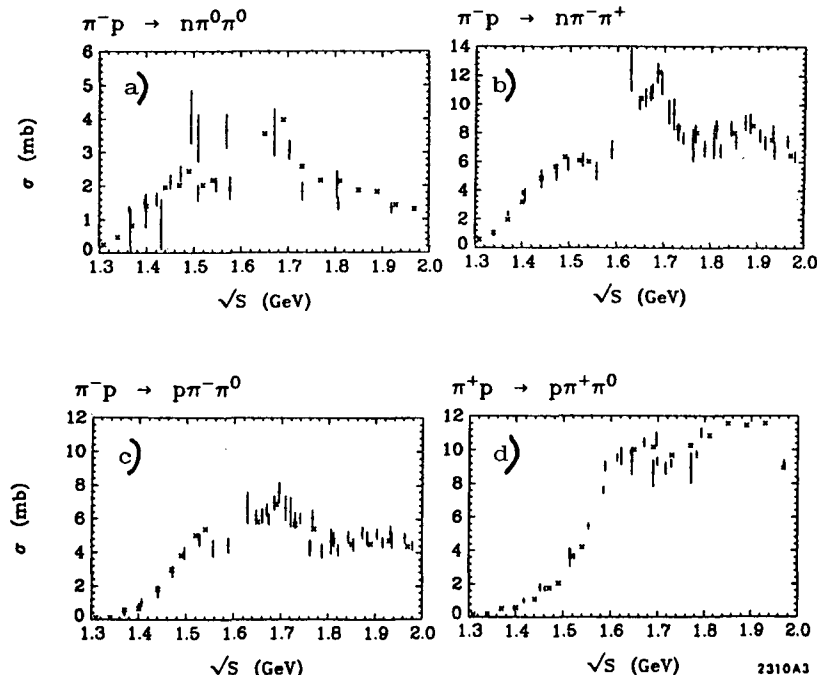


FIG. 6 -Single pion production cross sections. Data points are indicated by | and the predictions from our partial wave amplitudes by x.

6. RESULTS: ARGAND DIAGRAMS FOR 1972 SOLUTION ONLY

6.1 1972 vs. 1973 Solutions

Finally I can present some Argand Diagrams, but first a warning. As mentioned in Sect 5.1, paragraphs i) and iv), we are hampered by a gap in the available data between 1540 and 1650 MeV. Note on the figures following (7 through 12) that energy points M,N,O appear only on the elastic Argand plots, and note the energy gap in the inelastic T and $|T|^2$ plots.

We have found two solutions, which bridge this gap in different ways. One solution is old; we presented it at the 1972 Batavia Conference, and it is the only one for which I have Argand plots.

The other "1973" solution is still being explored. We found it only after considerable prodding and help by distraught theorists, mainly Gilman and Faiman. It has three more waves (ρ_1 PP_{11} - which Saclay decided independently should be included - ΔSP_{11} , and ΔFF_{15}), and a higher likelihood. All the big amplitudes are similar in both solutions, except for ΔPP_{11} , which is crucial for bridging the 1540 - 1650 MeV energy gap. The 1972 ΔPP_{11} amplitude moves fast at 1650 MeV (see Fig. 7), and (by continuity) also in the gap. So point R at 1690 MeV is nearly 180° out of phase with point K at 1520 MeV. The 1973 amplitude is motionless at 1650 (!), so continuity keeps the phase for the 1688 MeV region the same as at 1520. But PP_{11} is such a large wave, on both sides of the gap, that it influences all others. So the 180° difference between the 1972 and 1973 PP_{11} solutions produces a similar change in all other waves. I don't think we'll clear up this ambiguity until Saclay reports amplitudes (or events) in the gap.

6.2 Comments on selected Argand plots

On the Argand plots of Figs. 7,...11, the letters A through Z are the results of each single-energy fit, with statistical errors $\delta T \approx .03$ (twice the size of a letter). The magnitude of T comes directly from the fit. The phase has been calculated as discussed in Sect. 3, by a K-matrix fit to one or two large partial waves. In the region below 1540 MeV we used P_{11} ; above the 1540 to 1650 MeV gap we tied on to D_{15} and F_{15} ; in the 1920 region we rely on F_{35} .

The smooth Argand curves come from the K-matrix fits detailed in Lecture II. More details are given in the figure captions.

I include the following partial waves, with some comments on each:

- Fig. 7 (P_{11}). I have already mentioned the overwhelming importance of P_{11} in bridging the phase across the gap. Before this analysis EPSA told us that for the 1470 resonance $x_{e1} = \Gamma(\text{elastic})/\Gamma(\text{total})$ was about 50 %; for 1780, $x_{e1} \approx 15$ %. Now we see that the inelasticity at 1470 is due both to ΔPP_{11} ($x_{\Delta} \approx 30$ %) and ϵPS_{11} ($x_{\epsilon} \approx 25$ %). These estimates (and the signs) for many

reactions are in Table 2 of Lecture II.

- Fig. 8 (P_{13}). Here is an example of an inelastic resonance which is barely visible in the πN channel, because of its weak coupling. We now see it is mainly a ρN resonance; this was expected because it is seen strongly in photo-production.

- Fig. 9 (D_{13}), is visibly coupled to 5 decay channels. Two comments:-
i) There is a strong ρDS_{13} coupling although the $D_{13}(1520)$ is nearly 200 MeV below $N\rho$ threshold. Look at the clear ρN circle, and the B.W. shape of $|T_{\rho N}|^2$.
ii) A $D_{13}(1700)$ has been hinted at in EPSA ^{1,2)}, and now appears in both ϵN and $\Delta\pi$. This state is required to complete the N^* and $\Delta(70, 1^-)$ supermultiplet.

- Fig. 10 (D_{15}). I present this mainly for your inspection at the time that you read Sect. 6 of Lecture II. It is very clean (two good signals and little background) and was the first case in which we tested our ideas on Breit - Wigner "refits".

- Fig. 11 (F_{35}). This is the only case where we find that a Δ is seen only in the higher of the two L' states open to it, i.e. we see ΔFF_{35} , no ΔFP_{35} . This has been noted independently in the UCR/LBL ¹⁴⁾ single-channel ($\Delta\pi$) fit. F_{35} is the second, less "clean", resonance you will read about in Lecture II, Sect. 6 and Table 4, on Breit-Wigner "refits".

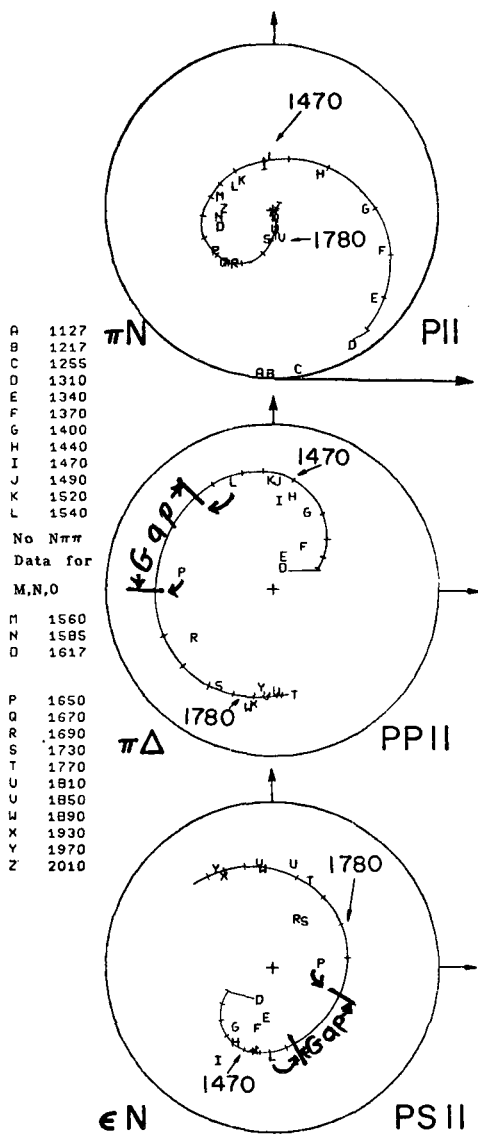
- Figs. 12 and 13. All inelastic waves are summarized in this Figure. The single-energy amplitudes have been joined by straight lines to guide the eye and tally the energy. But this creates a wrong impression across the gap from 1540 to 1650, which is too big an interval to join with a straight line. I have omitted the straight line but left the 5 arrows to indicate the gap.

NOTE ADDED JAN. 1974 (during publication): By now we are convinced that the 1973 Solution ("B") is the better, and Argand plots are of course available. I have added summary Argand plots of this solution in the form of Figs. 13 and 14. For more details see A. H. Rosenfeld et al., submitted to Phys. Rev. Letters, May 1974.

The presence of two P_{11} states at low energies (~ 1470 and ~ 1750) implies the need for two P_{33} states in most schemes, while the $[56, L=2^+]$ supermultiplet requires yet a third. There is evidence for one such state in EPSA at ~ 1900 MeV but there certainly is no such state in the region of 1700 MeV. The absence of these states at low energies, unless they have remarkably small πN , $\pi\Delta$, etc, couplings, or large mass splittings from their supermultiplet partners, must bring into question the present classification schemes.

We'll return to the Argand Plots in Lecture II.

Fig.7



P	1127
B	1217
C	1255
D	1310
E	1340
F	1370
G	1400
H	1440
I	1470
J	1490
K	1520
L	1540
No $N\pi\pi$	
Data for	
M,N,O	
H	1560
N	1585
D	1617
P	1650
R	1670
S	1690
T	1730
U	1770
V	1810
W	1850
X	1890
Y	1930
Z	1970
	2010

$I = \frac{1}{2} \pi N$ P11

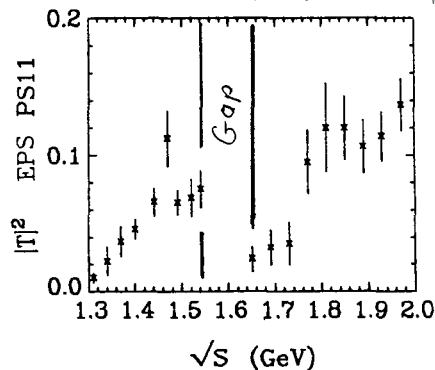
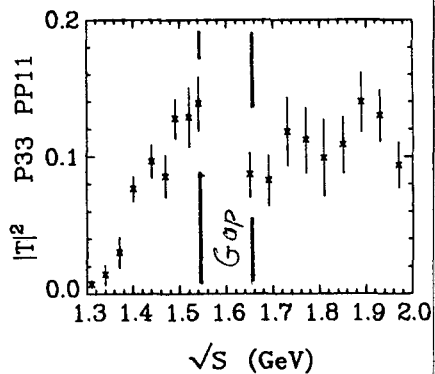
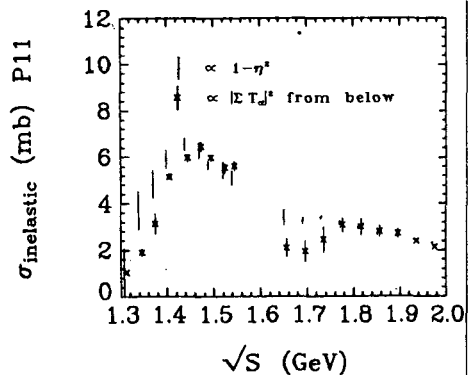
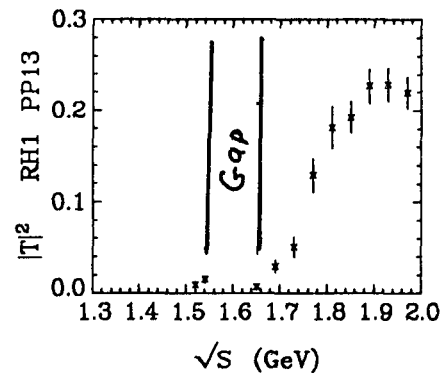
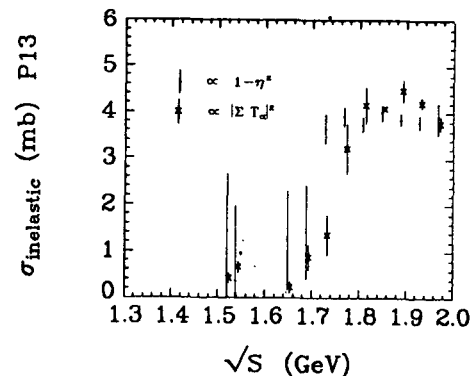
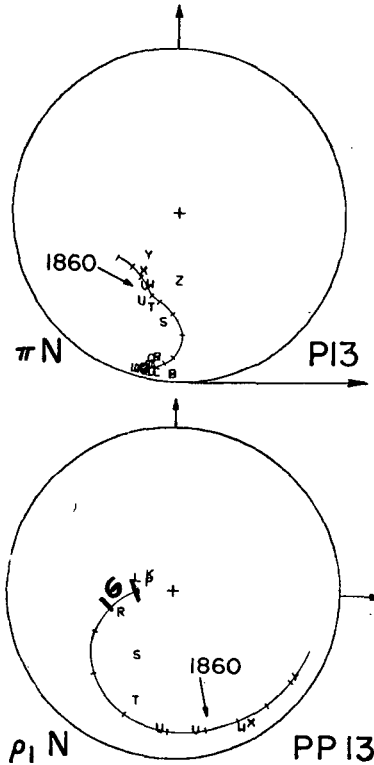


Fig.8

$I = \frac{1}{2} \pi N$ P13



Figs.7 through 11:- Argand Diagrams and partial wave cross sections for the elastic and inelastic channels. The smooth curve on the Argand Diagrams is the amplitude obtained from the K matrix when that description was possible. Cross-hatched marks on the curves correspond to the energies D,E,F, etc. The arrows indicate the known resonances from EPSA²). The total inelastic contribution in each elastic wave (ϕ) is compared with the sum of the inelastic contributions we observe. Facing each inelastic Argand diagram, we give the variation with energy of the square modulus of the wave.

A 1127
 B 1217
 C 1255
 D 1310
 E 1340
 F 1370
 G 1400
 H 1440
 I 1470
 J 1490
 K 1520
 L 1540
 No $\pi\pi\pi$
 Data for
 M,N,O
 H 1560
 N 1585
 O 1617
 P 1650
 Q 1670
 R 1690
 S 1730
 T 1770
 U 1810
 V 1850
 W 1890
 X 1930
 Y 1970
 Z 2010

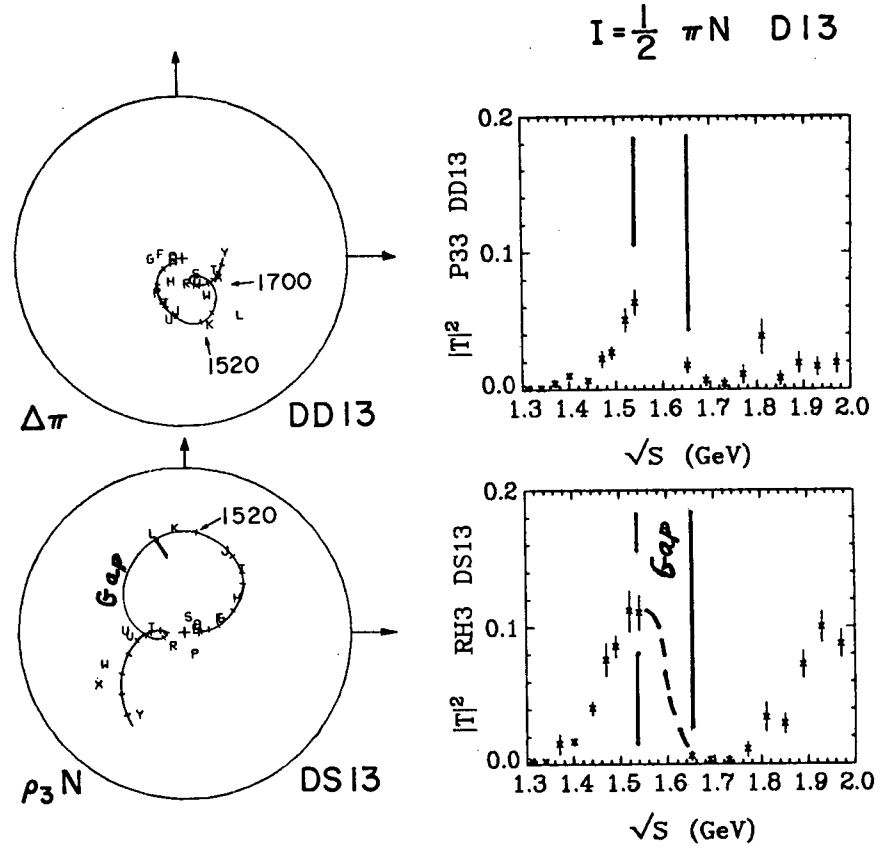
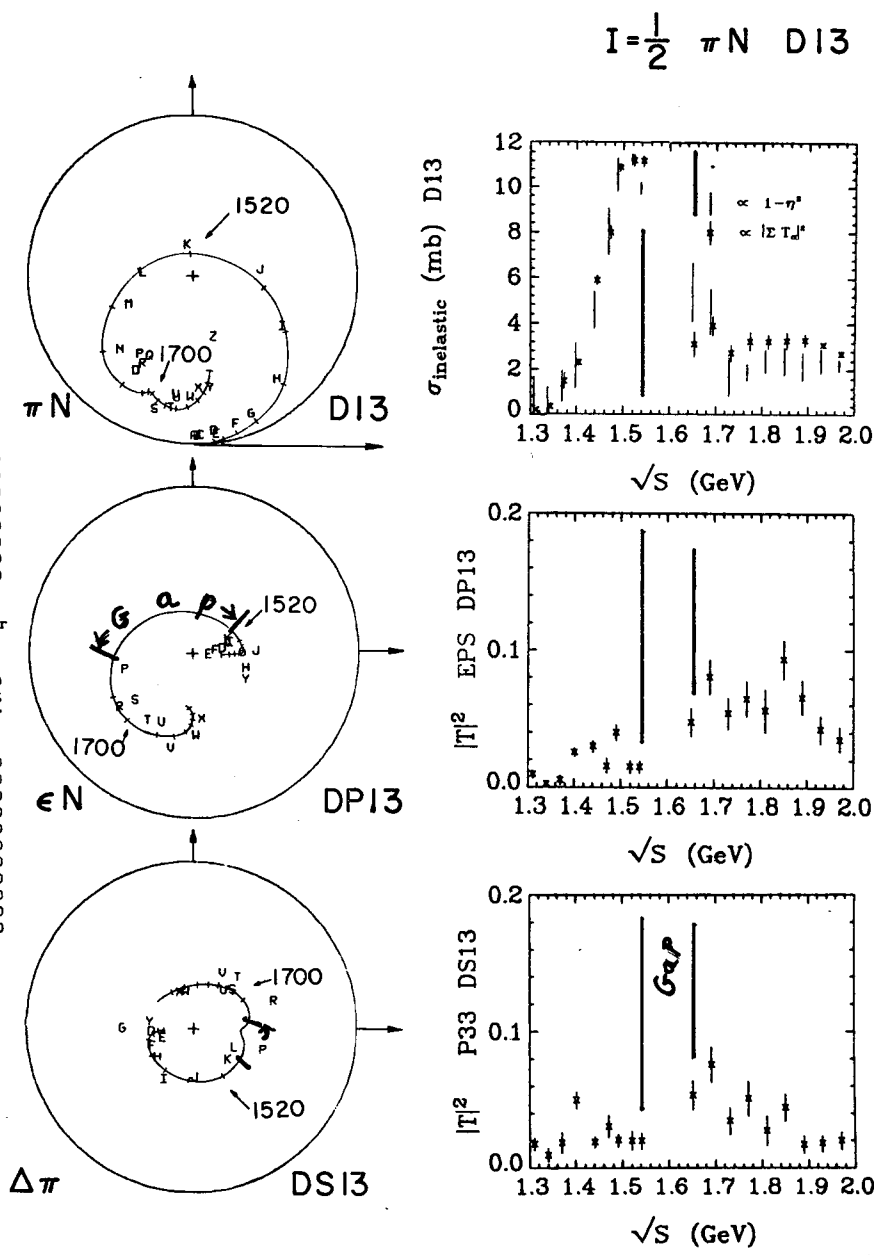


Fig. 9, see caption for Figs. 7,8.

Fig. 10

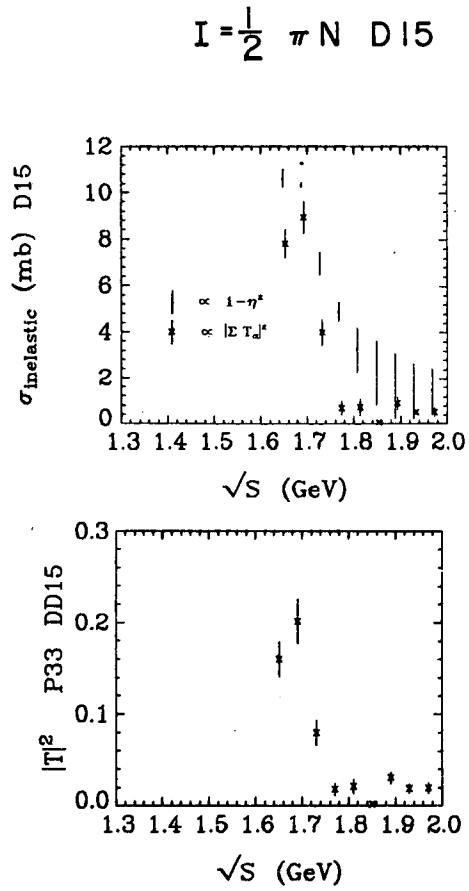
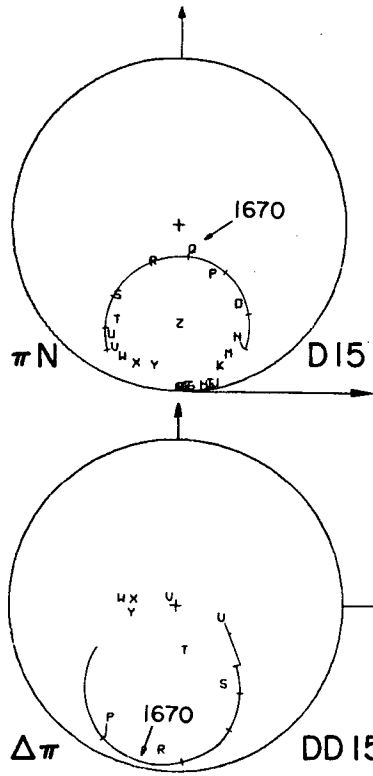
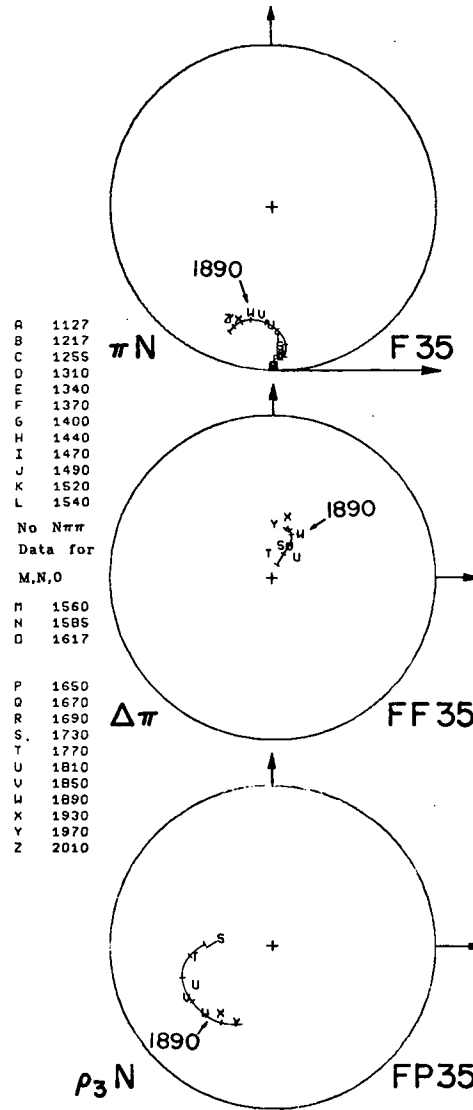
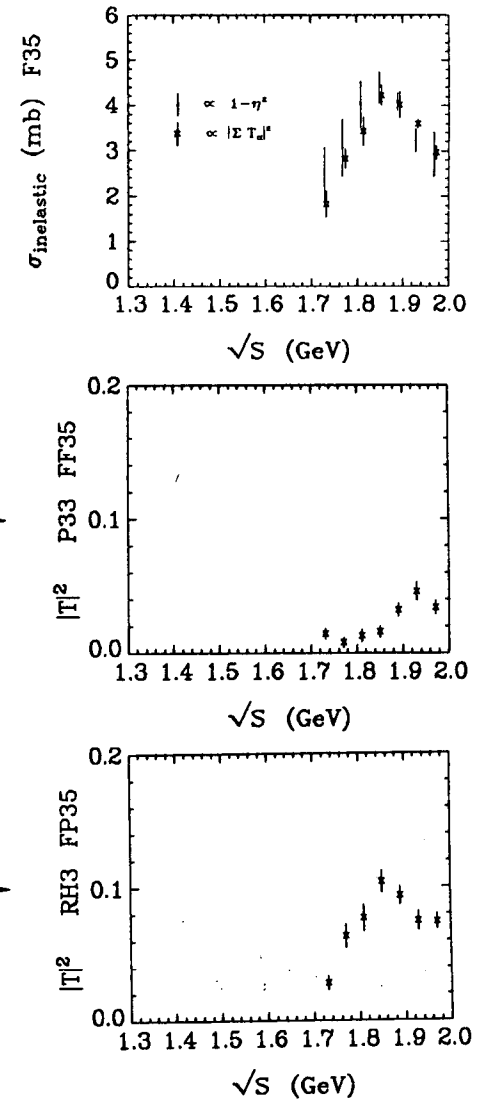


Fig. 11



D	1127
B	1217
C	1255
O	1310
E	1340
F	1370
G	1400
H	1440
I	1470
J	1490
K	1520
L	1540
No Nππ	
Data for	
M,N,0	
M	1560
N	1585
O	1617
P	
Q	1650
R	1670
S	1690
T	1730
U	1770
V	1810
W	1850
X	1890
Y	1930
Z	1970
	2010

$I = \frac{3}{2} \pi N$ F35



Figs. 10,11, see caption for Figs. 7,8.

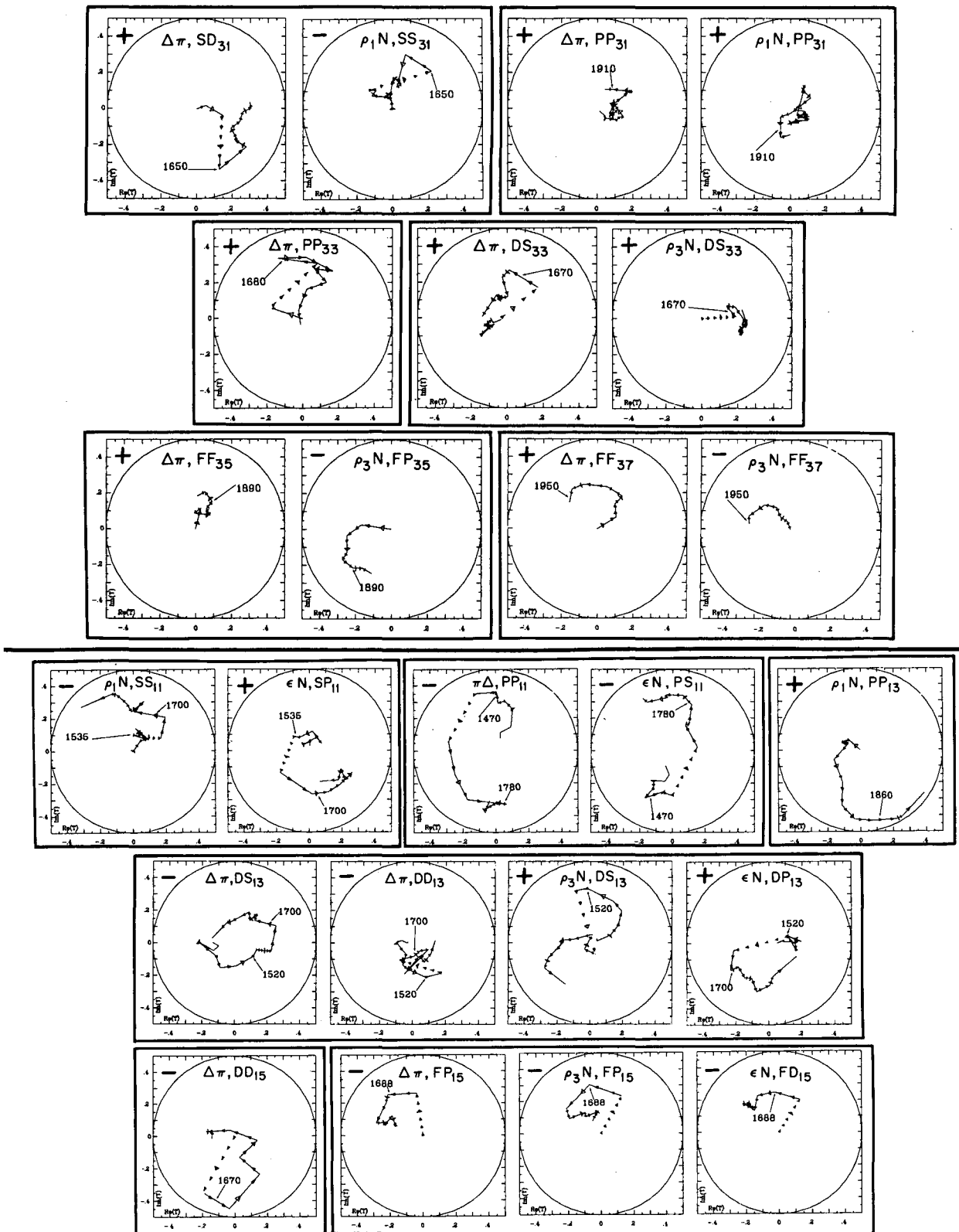


Fig. 12. Argand plots for Solution A (1972). The nominal energies come from the CERN 1972 partial wave analysis. Arrows on the Argand plots are spaced every 20 MeV, with wide arrows every hundred MeV; base of wide arrows mark integral hundreds of MeV. To show the 100-MeV gap in our data, the straight line joining the five gap arrows has been deleted. The + or - signs at the upper left of each circle show how to transform from our "internal" sign convention to the "Baryon-first" convention. Lower- ℓ curves are plotted starting at $\sqrt{s} = 1400$ MeV; higher- ℓ waves only where first needed in the fits. Last arrowhead is always at 1940 MeV.

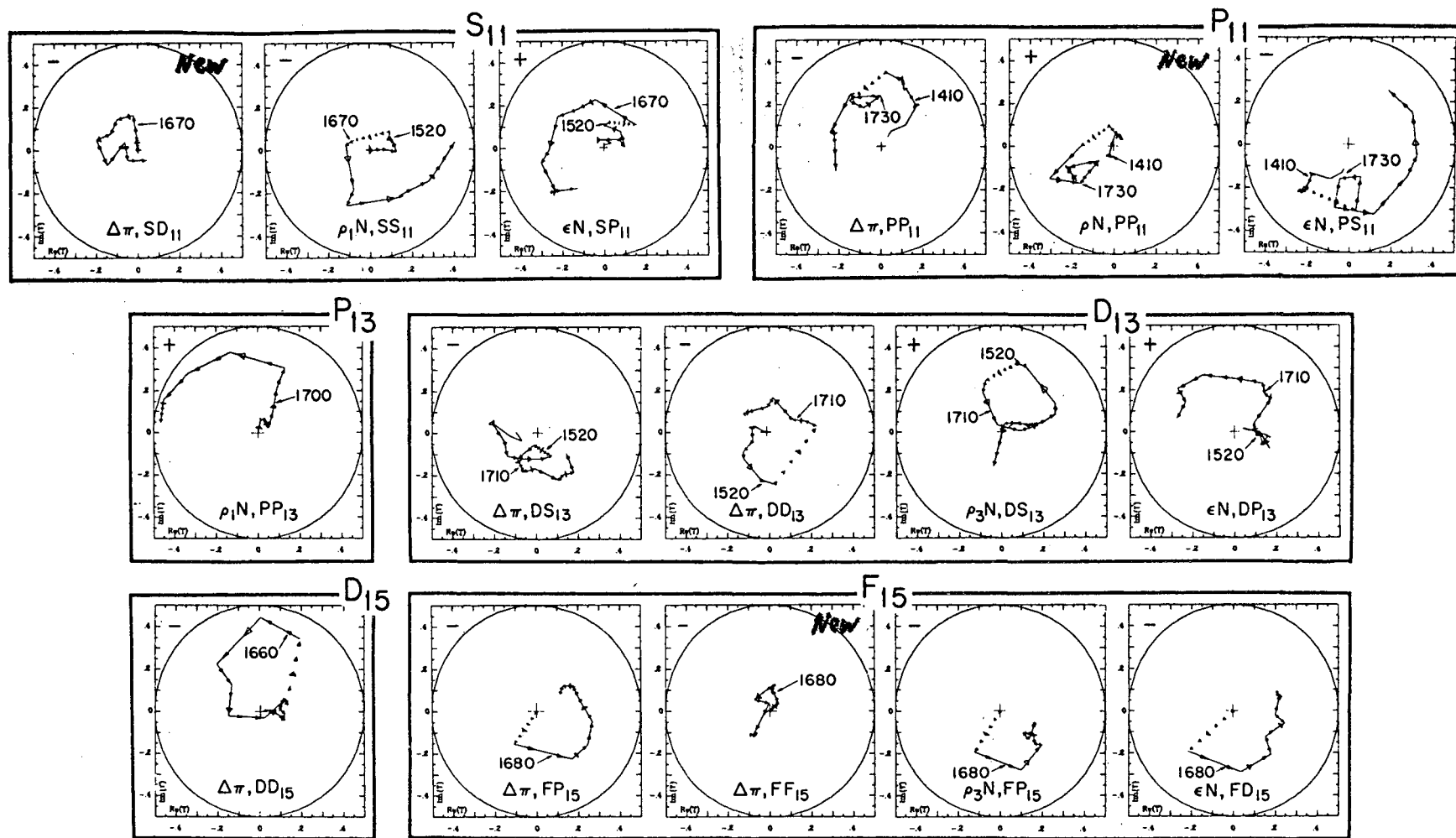
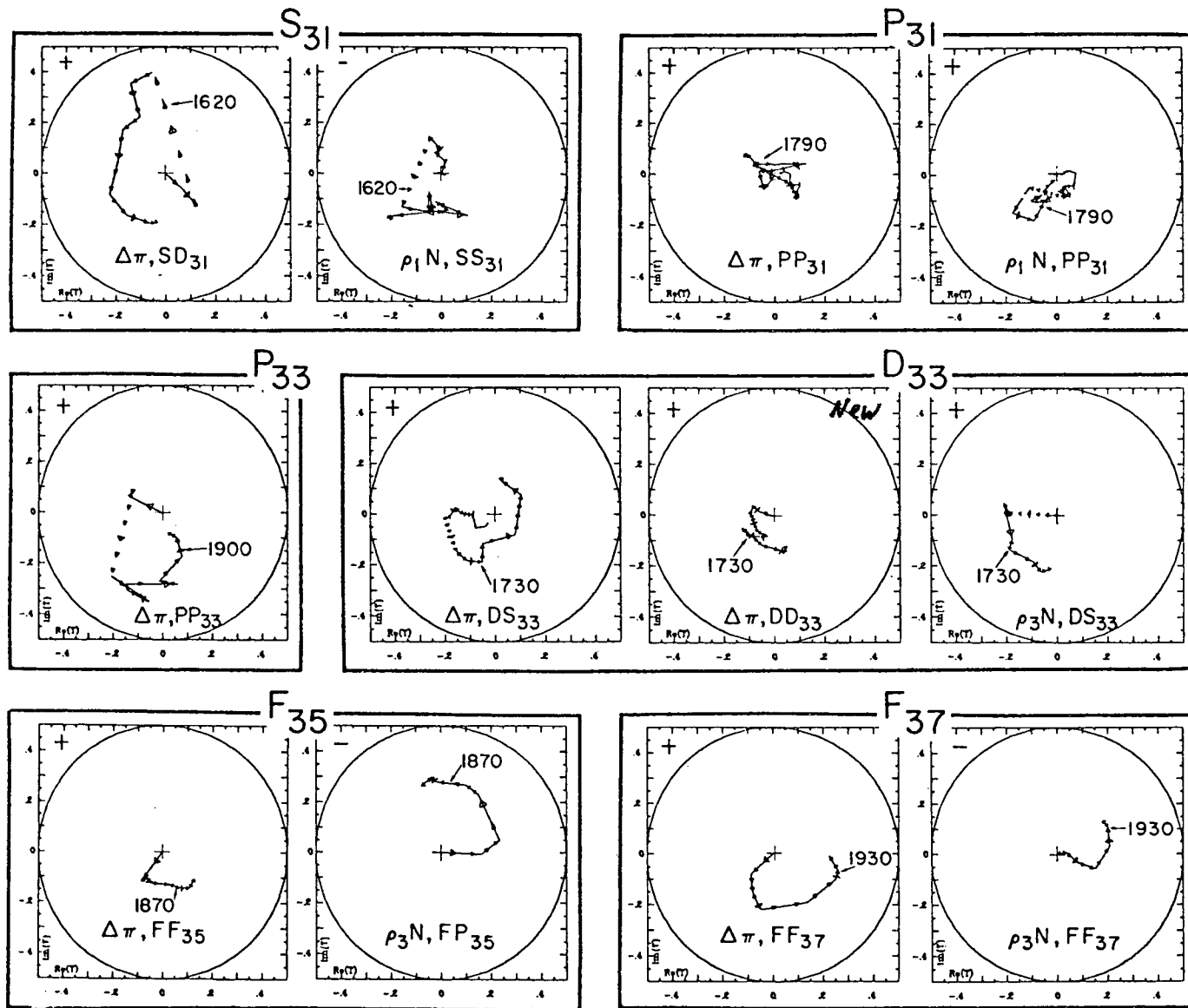


Fig. 13. Solution "B" (1973), $N\pi\pi$ Argand Plots. For these more modern plots, the 1973 Saclay EPSA solutions (Ref. 2) were available and have been used for the nominal resonance energies. Arrows are spaced every 20 MeV, with wide arrows every 100 MeV: base of wide arrows mark integral hundreds of MeV. Lower- ℓ waves are plotted starting at $\sqrt{s}=1400$ MeV; higher- ℓ waves only where they were first needed. Last arrowhead is always at 1940 MeV. To show the gap in our data the straight line joining the five gap arrows has been deleted. The + or - signs to the upper left of each circle show how to transform from our sign conventions to the "Baryon-first" convention.

XBL 741-2048



-20a-

Fig. 14. Solution "B", Argand Plots, continued for $I = 3/2$. See caption for Fig. 13.

REFERENCES FOR LECTURE I.

- 1) S. ALMEHED and C. LOVELACE Nucl. Phys. B40, 157 (1972).
- 2) R. AYED, P. BAREYRE, Y. LEMOIGNE, contributed paper to the XVI International Conference on High Energy Physics, Batavia (1972).
- 3) For complete photoproduction references see the Particle Data Group's latest annual Review of Particle Properties e.g. reference 4.
- 4) Particle Data Group, Rev. Mod. Phys. 45, N°2 Part II, (1973).
- 5) B. DELER and G. VALLADAS, Nuovo Cimento 45A, 559 (1966).
- 6) R.J. CASHMORE, D.J. HERNDON, and P. SÖDING, LBL-543 (unpubl. 1973).
- 7) A.D. BRODY and A. KERNAN, Phys. Rev. 182, 1785 (1969).
- 8) M.G. BOWLER and R.J. CASHMORE, Nucl. Phys. B17, 331 (1970).
- 9) W. CHINOWSKY, J.H. MULVEY, and D.H. SAXON, Phys. Rev. D2, 1790 (1970).
- 10) For the latest in a long series of Saclay papers, see J. DOLBEAU and F. TRIANTIS, Paper Submitted to the 2nd Aix-en-Provence Conference on Elementary Particles, 1973. This is based on an entirely new computer program which yields both the phase and magnitude of the amplitudes. For older analyses of magnitude only, see several theses:-
NGUYEN THUC DIEM, Thesis, note CEA N-1602, Paris (1972);
P. CHAVANON, Collège de France, Thesis (1971).
- 11) D.J. HERNDON, R. LONGACRE, L.R. MILLER, A.H. ROSENFELD, G. SMADJA, P. SÖDING, R.J. CASHMORE, D.W.G.S. LEITH, LBL-1065/SLAC-PUB-1108 (1972), submitted to Phys. Rev. as LBL 1065 (Rev.) Sept. 1973.
- 12) K.M. WATSON, Phys. Rev. 88, 1163 (1952).
- 13) A.D. BRODY, R.J. CASHMORE, A. KERNAN, D.W.G.S. LEITH, B.G. LEVI, B.C. SHEN, D.J. HERNDON, L.R. PRICE, A.H. ROSENFELD, P. SÖDING, Phys. Letters 34B, 665 (1971).
- 14) V. MEHTANI, S.Y. FUNG, A. KERNAN, T.L. SCHALK, Y. WILLIAMSON, R.W. BIRGE, G.E. KALMUS and W. MICHAEL, Phys. Rev. Letters 29, 1634 (1972);
- 15) G. SMADJA, "Resonances that Overlap" LBL-382 (unpublished 1971).
- 16) R. OMNES, Nuovo Cimento 8, 316 (1958).
- 17) A. BERTHON, L. MONTANET, E. PAUL, P. SAETRE, A. YAMAGUCHI (CERN) and G. BURGUN, E. LESQUOY, A. MULLER, E. PAULI, F.A. TRIANTIS, S. ZYLBERAJCH (CEN, Saclay); CERN Preprint D.Ph.II/PHYS 73-31, submitted to the IIInd Aix-en-Provence Conference on Elementary particles, 1973.
- 18) R.J. CASHMORE, SLAC-PUB - 1257 and Proc. Purdue Conference on Baryon Resonances (1973).
- 19) L.R. MILLER, Ph.D. Thesis, LBL-38 (unpublished).
- 20) D.J. HERNDON, Thesis, LBL-544 (unpublished, 1972).

LECTURE II: FROM ARGAND DIAGRAMS TO PHYSICS

In this lecture I shall discuss some physics which we can learn from the Argand plots explained and presented in Lecture I.

This lecture has separately numbered figures, tables, and references, because I want to use part of the lecture as a contribution to the forthcoming (Sept. 73) conference at Aix-en-Provence.

1. COMPARISON OF $\gamma P \rightarrow \pi N$ AND $\pi N \rightarrow \rho N$ WITH THE QUARK MODEL

In sections 2 and 3 of this lecture I shall take up various higher-symmetry tests of $\Delta\pi$ amplitudes; first I want to dispose of γN and ρN .

SU(3) tests of (Vector Meson) \times (Nucleon) would need analyses such as $K^-p \rightarrow K^*N$ or ρY , and I am not aware of any relevant results.

γN and ρN can be compared either:-

- a) directly, using the notions of vector dominance, or
- b) separately, each with the quark model or SU(6).

For a) we must transform our partial-wave amplitudes $T(J^P, L, L')$ with a 3×3 matrix into helicity amplitudes which are conventional for photon reactions: call them $T(\lambda = \frac{1}{2})$, $T(\lambda = \frac{3}{2})$, and the unobservable T for longitudinal photons. In our analysis we have yet to propagate all the errors through this transformation, so I shall say no more at present.

I take up next the direct comparisons, b).

1.1 γN vs. the Quark Model

At LBL, Moorhouse and Oberlack¹⁾ have recently done a partial-wave analysis of photoproduction, and have found really encouraging agreement with the quark model. Fig. II-1 is just a photograph of their summary table.

To make a stringent comparison with the quark model we may take only the larger couplings of the prominent resonances, and only those where quark model predictions are "starred" in Fig. 1. We find seven such cases, underlined in Fig. 1, where the experimental sign is sure and which theoretically depend on, and only on, the Clebsch-Gordan coefficients of the quark model (the same in either the "relativistic" or "nonrelativistic" models). These 7 signs all agree! About 7 more signs which are less certain also agree [but not those for $P_{11}(1470)$] and in general all 33 magnitudes agree within a factor of 3. I remind you that the chance of random agreement of say 10 signs is $2^{-10} \approx 10^{-3}$, so I consider this to be an impressive systematic test of the quark model.

Fig. II-1. Comparison of pion photoproduction amplitudes with Quark Model. This a reproduction of Table 1 of Moorhouse and Oberlack (Ref. 1).

Average resonance couplings from seven fits to the data compared with quark-model predictions. The result from the partial wave analysis is an average over seven fits and the error is the spread over the seven fits; directly underneath the partial wave analysis result we give the quark-model result for the usual assignment of the resonance to an $\{SU_6\}L, [SU_3, 2S+1]$ multiplet. An asterisk denotes that the quark-model result does not involve a difference of two terms. Table 1a comprises resonances assigned to the $\{56\}L=0^+$ and $\{70\}L=1^-$ multiplets and table 1b the $\{56\}L=2^+$, $\{56\}_2L=0^+$ and $\{70\}_2L=0^+$ multiplets where the suffix denotes radial excitation. In table 1b we also give quark-model results for some resonances for which we do not have partial wave results since they are outside our data range. $A_{1/2}$ and $A_{3/2}$ denote decays through helicity-1/2 and helicity-3/2 states, respectively, and superscripts + and 0 denote decays of charge +1 and charge 0 particles respectively. Units are $\text{GeV}^{-1/2} \times 10^{-3}$.

Table 1a					Table 1b					
$N^*(\text{mass})$ $[SU_3, 2S_{\text{quark}}+1]J^P$	$A_{1/2}^+$	$A_{3/2}^+$	$A_{1/2}^0$	$A_{3/2}^0$	$N^*(\text{mass})$ $[SU_3, 2S_{\text{quark}}+1]J^P$	$A_{1/2}^+$	$A_{3/2}^+$	$A_{1/2}^0$	$A_{3/2}^0$	
$\{56\}L=0^+$	$p_{33}(1230)$	-142 ± 6	-259 ± 16			$[8, 2] 3/2^+$	-11	30	30	0^*
	$[10, 4] 3/2^+$	-108^*	-187^*	etc		$f_{15}(1690)$	-8 ± 4	100 ± 12	17 ± 14	-5 ± 18
	$s_{11}(1545)$	53 ± 20		-48 ± 21		$[8, 2] 5/2^+$	-10	60^*	30^*	0^*
	$[8, 2] 1/2^-$	156		-108		$[10, 4] 1/2^+$	-30			
	$d_{13}(1512)$	-26 ± 15	194 ± 31	-85 ± 14	-124 ± 13	$[10, 4] 3/2^+$	-30	50		
	$[8, 2] 3/2^-$	-34	109^*	-31	-109^*	$f_{35}(1870)$	$-60 \pm ?$	$-100 \pm ?$		
	$s_{31}(1620)$	90 ± 76				$[10, 4] 5/2^-$	-20	-90		
	$[10, 2] 1/2^-$	47				$f_{37}(1950)$	-133 ± 46	-100 ± 41		
	$d_{33}(1635)$	68 ± 42	22 ± 52			$[10, 4] 7/2^+$	-50^*	-70^*		
	$[10, 2] 3/2^-$	88	84^*							
$\{70\}L=1^-$	$s_{11}(1690)$	66 ± 42		-72 ± 66		$\{56\}_2L=2^+$				
	$[8, 4] 1/2^-$	0		-30		$\{56\}_2L=0^+$	$p_{11}(1470)$	-55 ± 28		2 ± 25
	$d_{13}(1700)$	$3 \pm ?$	$20 \pm ?$	$-28 \pm ?$	$27 \pm ?$	$\{70\}_2L=0^+$	$[8, 2] 1/2^+$	27		-18
	$[8, 4] 3/2^-$	0^*	0^*	10^*	-40^*		$p_{11}(1750)$	26 ± 28		27 ± 22
	$d_{15}(1670)$	11 ± 12	21 ± 20	10 ± 40	-35 ± 14		$[8, 2] 1/2^+$	-40		10
$[8, 4] 5/2^-$	0^*	0^*	38^*	-53^*						

1.2 ρN vs. the Quark Model

Very recently, Moorhouse and Parsons²⁾ have made the same quark model comparison for the photon's heavy relative, the rho meson, using our amplitudes for $N \rightarrow I(J^P) \rightarrow \rho N$. Alas, neither the length of the table nor its contents are quite so impressive, so I shall not reproduce it. There are only 3 "starred" predictions, and they are indeed satisfied by our amplitudes. In addition there is an unstarred prediction for ρ_{35}^{FP} which does not agree with our solution. Another starred prediction awaits the bridging of the Saclay gap. Tune in later for more details.

2. $SU(3)$ TESTS: $\pi N \rightarrow \Delta \pi$ vs $\bar{K} N \rightarrow \Sigma(1385)\pi$.

It is well known that one of the major triumphs of $SU(3)$ has been the agreement between "isoscalar coefficients" c_i and experimental signs for amplitudes $T_{1\alpha}$ for reactions like

$$\begin{aligned}
 K^- p \rightarrow \left(\frac{3^-}{2} \text{ nonet}\right) \rightarrow \bar{K}N; & \quad T_{11} \propto g_1^2 c_1 c_1 \\
 & \rightarrow \Sigma\pi; \quad T_{12} \propto g_1^2 c_1 c_2 \\
 & \rightarrow \Lambda\pi; \quad T_{13} \propto g_1^2 c_1 c_3
 \end{aligned} \tag{1}$$

According to SU(3) these are all examples of elastic scattering with a coupling constant g (actually g_D and g_F but let's ignore that annoyance), so the coefficients c_i are just generalizations of Clebsch-Gordan coefficients. So far, about six SU(3) multiplets are established (2 nonets, 2 octets, 2 decuplets) which satisfy about 20 sign checks. I repeat that this cannot just be good luck because $2^{-20} \approx 10^{-6}$.

Now we can compare our amplitudes for $\pi^- p \rightarrow \left(\frac{3^-}{2}, \frac{5^-}{2}, \text{ and } \frac{5^+}{2}\right) \rightarrow \Delta\bar{\pi}$ with a CHS analysis³⁾ of $\bar{K} p \rightarrow (\text{same}) \rightarrow \xi(1385)\bar{\pi}$. The relative signs of the two $J=\frac{5}{2}$ waves agrees with SU(3); the sign for DD_{13} if we chose our 1973 solution.

3. COMPARISON OF $\Delta\pi$ AMPLITUDES WITH SU(6) AND QUARK MODEL

In SU(6) the nucleon and Δ belong to the same 56 supermultiplet, so elastic scattering generalizes to reactions like

$$\begin{aligned}
 \pi N \rightarrow (\underline{70}, L^P = 1^-) \rightarrow N\pi; & \quad T_{11} \propto g_1^2 c_1^2 \\
 \text{and} & \quad \rightarrow \Delta\pi; \quad T_{12} \propto g_1^2 c_1 c_2.
 \end{aligned} \tag{2}$$

We have to "waste" one reaction to define the overall phase (and thus the sign of c_2/c_1), but then the other reactions via the same $\underline{70} \rightarrow \underline{56} \times \underline{\pi}$ serve as sign checks. Unfortunately, just as in SU(3) there were really two couplings ($g = g_F + g_D$), so in SU(6) there are again two for the $\Delta\pi$ case, this time because of the fact that a resonance can decay into $\Delta\pi$ via two different values of L' (e.g. $D_{13} \rightarrow \Delta DD_{13}$ and ΔDS_{13} , see Sect. 4a. of Lecture I).

It is the open choice of the relative sign of the two L' couplings which leads to the two alternative columns of Table 1, labelled either:

Faiman-Rosner	$\rightarrow "SU(6)_w"$	$"Anti-SU(6)_w"$
Gilman-Kugler-Meshkov	$\rightarrow "(8,1)_0 - (1,8)_0"$	$"(3,\bar{3})_1 - (\bar{3},3)_{-1}"$

The Faiman-Rosner names are old, based on the argument about the two different values of L' . The group-theoretical names come from the transformations studied by Melosh⁴⁾ who showed that indeed there are two couplings, with those two transformation properties. Note on Table 1, however, that the Quark Model does not put up with this ambivalence -- it predicts a unique column, which corresponds to the Anti-SU(6) choice.

Table II-1

Signs of the amplitudes for $\pi N \rightarrow N^* \rightarrow \pi \Delta$ for N^* 's in the $\underline{70}$ $L = 1$ and $\underline{56}$ $L = 2$. Products of the theoretical and experimental signs for decays through the $(8, 1)_0 - (1, 8)_0$ and $(3, \bar{3})_1 - (\bar{3}, 3)_{-1}$ terms are presented, with the overall phase chosen so that DD13(1520) is positive. Signs which are independent of which term dominates are denoted by a "*" . Experiment and theory agree if within the $\underline{70}$ $L = 1$ or $\underline{56}$ $L = 2$ decays all the signs in a column agree.^{a)}

Faiman-Rosner ⁵⁾	\longrightarrow	$SU(6)_w$	$Anti-SU(6)_w$	Moorhouse ²⁾ and Parsons quark model
Gilman-Kugler-Meshkov ⁶⁾	\longrightarrow	$(8, 1)_0 - (1, 8)_0$	$(3, \bar{3})_1 - (\bar{3}, 3)_{-1}$	
$\underline{70}$ $L=1 \rightarrow \underline{56}$ $L=0$	$\left\{ \begin{array}{l} DD13(1520) \\ DS13(1520) \end{array} \right.$	+	+	+
		-	+	+
	$\left\{ \begin{array}{l} SD31(1640) \\ DS33(1690) \\ DS13(1700) \\ DD15(1670) \end{array} \right.$	+	-	? b)
		+	-	? b)
		+	- ? c)	? b)
		-*	-*	-*
	$\underline{56}$ $L=2 \rightarrow \underline{56}$ $L=0$	$\left\{ \begin{array}{l} FP15(1688) \\ FF35(1880) \\ FF37(1950) \end{array} \right.$	-	+
-*			-*	-*
-*			-*	-*

} Energy^{a)} gap
} Only disagree-
ment

a) Because of experimental inability so far to bridge 100 MeV gap between 1520 region and 1688 region, signs so far need not check across this gap.

b) Moorhouse's "?" means he feels the experiment is uncertain.

c) ? in $Anti-SU(6)_w$ column means we feel experiment is uncertain.

Table II - 1 is taken from Gilman et al.⁶⁾ (but Faiman and Rosner give the same prediction); it gives the product of theoretical signs with our experimental signs for our 1972 solution. (For our 1973 solution change the two signs below the energy gap with respect to the 7 signs above). We see that the theorists badly need our 1973 solution (in fact they helped us find it). Only for that solution can one find a complete column of minus signs, by choosing $Anti-SU(6)$ for $\underline{70}$ decays and $Straight-SU(6)$ for $\underline{56}$ decays. As usual, tune in again after Saclay helps us bridge the gap.

4. ESTIMATING RESONANCE PARAMETERS "BY EYE", WITHOUT A K-MATRIX.

We are through with the glamorous problem of signs and higher symmetries. The rest of this lecture deals with a more pedestrian question: "Is there a reliable way to parametrize a resonance?" We shall exploit our multichannel amplitudes to find two consistent descriptions, which are compared in Table 4. But be careful: some partial widths will differ by a factor two, depending in which description you chose.

Before we go on to Fancy Method I (K-matrix fits and T-matrix poles), I present in Table 2 the most conventional method of all --- "eye-ball" fits to the Argand plots of Lecture 1 according to the following recipe:-

1) We look at all Argand plots coupled to a given incoming partial wave (e.g. all three P_{11} channels of Fig. 7 of Lecture I), giving the most weight to the ones which look most resonant, and pick an energy where they all simultaneously seem to have the greatest speed. This is called the resonance energy. We then draw semi-circles through the points near the greatest speed, and estimate the radius r of each circle. Then $r = \sqrt{X_{e1} X_{\alpha}}$ (see below).

2) We get help from Elastic Phase Shift Analyses (EPSA, Refs. 7 and 8) in two ways:

a) The Argand plots have already had their phases set to agree with some resonance seen strongly in EPSA -- e.g. P_{11} near 1520 MeV (see Lect. I, Sect. 6.2).

b) We use the EPSA values of Γ_{tot} and X_e in order to calculate X_{inel} . The numbers appearing in Table 2 in each inelastic channel are $\sqrt{X_{e1} X_{inel}}$ and (below that) Γ_{inel} ; the final column corresponds to the sum of the branching fractions for the given resonance. It should be noted that X_{inel} are very sensitive to variation in the X_{e1} , the elastic branching fraction.

Finally, one might note that in many cases all decay modes of the resonance are essentially accounted for ($\sum X_i \approx 1$).

Table II-2

Resonance couplings estimated by eye for $N\pi\pi$ channels, with help from EPSA^{7,8}). Each entry contains the partial wave considered, the amplitude at resonance and the partial width in MeV.

Resonance	E (MeV)	Γ_{tot} (MeV)	x_{el}	$\pi\Delta$	$\pi\Delta$	$N\rho_3$	$N\rho_1$	$N\epsilon$	Σx_i
P11	1440	236	.52 124	PP11 +.29 36				PS11 -.25 28	.80
D13	1520	119	.57 68	DS13 -.27 15	DD13 -.21 9.0	DS13 +.31 20.0			.94
S31	1630	160	.32 51	SD31 -.325 52			SS31 +.307 47		.95
D15	1670	141	.40 56	DD15 -.46 75					.93
F15	1690	133	0.6 80	FP15 +.31 21		FP15 +.27 16		FD15 +.24 13	.97
D33	1670	207	0.16	DS33 +.37 172					.99
S11	1700	148	0.50 74				SS11 +.19 11	SP11 -.35 35	.81
D13	1730	130	0.10 13	DS13 +.11 17				DP13 -.29 109	1.07
P11	1750	183	.15 28	PP11 -.345 140				PS11 +.21 52	1.21
P13	1850	250	.25 63				PP13 -.44 195		1.03
F35	1890	260	.15 40		FF35 +.10 16	FP35 -.29 140			.75
F37	1930	230	.40 92	FF37 +.25 36		FF37 -.25 36			.71

5. MULTICHANNEL K-MATRIX AND T-MATRIX FITS

Our ability to account for all of the πN inelasticity in many partial waves indicates that we are now in the position to perform multichannel fits, exploiting the constraints of unitarity to their fullest possible extent, in attempting to understand the πN interaction.

For this purpose we used a K matrix to parametrize our T-matrix elements obtained from our isobar model fitting program.

It is well known that for a partial wave which is coupled to several particle states, a real K matrix can be related to the Argand amplitudes by¹⁰⁾

$$T_{ij} - K_{ij} = i \sum_l T_{il} Q_l K_{lj}, \quad (3)$$

where the Argand amplitude is related to T by

$$A_{ij} = Q_i^{1/2} T_{ij} Q_j^{1/2} \quad (4)$$

and Q is a diagonal matrix corresponding to the c. m. momentum of the particles in each channel.

We now can make a reduced K-matrix equation by putting in the barrier penetration factors. We let

$$\begin{aligned} K_{ij} &= B_i^{1/2} k_{ij} B_j^{1/2}, \\ T_{ij} &= B_i^{1/2} \tau_{ij} B_j^{1/2}, \end{aligned} \quad (5)$$

where B is the Blatt-Weisskopf¹¹⁾ barrier factor. Thus Eq. (3) becomes

$$\tau_{ij} - k_{ij} = i \sum_l \tau_{il} Q_l B_l k_{lj} \quad (6)$$

and Eq. (4) becomes

$$A_{ij} = Q_i^{1/2} B_i^{1/2} \tau_{ij} Q_j^{1/2} B_j^{1/2}. \quad (7)$$

In order to extend this prescription to isobars which do not have a fixed mass, we replace $Q_l B_l$ by their weighted average value $\overline{Q_l B_l}$, where $\overline{Q_l B_l}$ is defined by the integration of $Q_l B_l$ over a normalized Dalitz plot projection of this isobar's diparticle mass¹²⁾.

Because the isobars are not an orthogonal set, they have an overlap with respect to one another. So off-diagonal terms will enter into the momentum matrix. Thus Eq. (6) becomes

$$\tau_{ij} - k_{ij} = i \sum_{lm} \tau_{il} \Delta_{lm} k_{mj}, \quad (8)$$

where Δ_{lm} for the diagonal terms are

$$\Delta_{11} = \overline{Q_1 B_1} \quad (9)$$

and the off-diagonal terms are related to the overlaps between the isobar states.

The reduced K matrix is then parametrized by simple factorizable poles and linear background terms which are not factorizable. These parameters are then adjusted to fit the Argand amplitudes. The resulting K-matrix parameters yielded "ridiculous" values for the masses and partial widths of the resonances (i. e., if interpreted literally they correspond to resonances which are shifted by ~ 100 MeV from their nominal value and have much greater widths than expected from inspection of the Argand diagrams). This is not surprising, the K-matrix is merely a good way to parametrize the T-matrix in terms of real numbers, and K-matrix pole positions and residues even change along with the number of channels considered.

5.1 Poles of the T-matrix

If we have a good representation of the Argand diagrams, this implies that we have a comparatively good description of the T matrix as a function of energy. In order to identify resonances and their properties we now search the T matrix for poles in the complex energy plane and determine the residues at these poles. The motivations for this procedure are:

- i) we expect the pole positions and residues in the T matrix to be independent of our parametrization of the T matrix, providing, of course, that it is good. This expectation stems from the work on the P33(1236) resonance.^{13, 14)} and investigation of our own¹²⁾;
- ii) we expect the pole position and residue to be closely related to the Breit-Wigner parameters but the pole position does not equal M_0 , $1/2 \Gamma_0$, the conventional Breit-Wigner parameters, and the residues are not necessarily equivalent to the widths. We expect these equalities to become very poor when we either have large backgrounds or wide resonances.

The results of these investigations are contained in Table 3, where we give the real and imaginary parts of the pole position together with the residues of the $\tau_{\alpha\alpha}$ matrix scaled by $2 \times \overline{Q_\alpha B_\alpha}$ calculated at an energy $E = \text{Real}(E_{\text{pole}})$. These will correspond to the partial widths, and the residues of the τ matrix correspond to the couplings. Several comments about these results are in order:

- i) often the pole positions are a long way from the position one might expect, e. g., F35, F37, or P13;
- ii) $1/2 \sum |\Gamma_i| \neq -\text{Im}(E_{\text{pole}})$ in many cases (where Γ_i is given by $\Gamma_i = 2 \times \overline{Q_i B_i} (\text{res}_i)^2$). However, it should be noted that even a pure Breit-Wigner will not have this property. The way we have defined Γ_i gives the closest agreement with the equality for a pure Breit-Wigner¹²⁾.

If the background becomes large, the disagreement becomes worse.

- iii) The last point is further emphasized by the fact that the residues have large phases even after taking into account the phases associated with the kinematical factors.

Table II-3

T-matrix poles and residues. Partial widths Γ_i are calculated by $\Gamma_i = 2 \times Q_i B_i$ (evaluated at $E = \text{Re } E(\text{pole})$) (residue $_i$)². Entries for Γ_i are $\Gamma_{\text{real}} / \Gamma_{\text{imag.}} / |\Gamma|$ in MeV.

Wave	Pole	$\Gamma_{\pi N}$	$\Gamma_{\pi\Delta_L}$	$\Gamma_{\pi\Delta_L'}$	$\Gamma_{N\rho_3}$	$\Gamma_{N\rho_1}$	$\Gamma_{N\epsilon}$	Other channel	$\Gamma_{\text{tot}} = \Sigma \Gamma_i $
S11	$1503 - i\frac{65}{2}$	7				6	23	2	67
		-6				0	35	10 (ηN)	
		9				6	42	10	
	$1652 - i\frac{100}{2}$	26				-3	-2	5	91
		-37				-9	-4	-32 (ηN)	
		45				9	5	32	
P11	$1385 - i\frac{235}{2}$	36	21				5		155
		-109	-25				-5		
		115	33				7		
	$1724 - i\frac{283}{2}$	-39	47				31		233
		-115	5				-56		
		122	47				64		
P13	$1728 - i\frac{159}{2}$	1				42			109
		-25				-73			
		25				84			
D13	$1514 - i\frac{142}{2}$	88	5	3	34		-3		176
		13	36	14	6		0		
		89	36	14	34		3		
	$1647 - i\frac{117}{2}$	5	-8	0	-1		-57		111
		-15	-22	-2	4		-32		
		16	24	2	4		65		
D15	$1666 - i\frac{159}{2}$	68	91						161
		-14	-10						
		69	92						
F15	$1672 - i\frac{155}{2}$	99	5		33		15		182
		-17	11		-27		-16		
		101	12		42		21		
S31	$1600 - i\frac{79}{2}$	-3	22			-5			149
		-20	16			102			
		20	27			102			
D33	$1657 - i\frac{109}{2}$	7	-9		36				95
		-4	-49		9				
		8	50		37				
F35	$1824 - i\frac{282}{2}$	36	19		-20				177
		-26	-18		-105				
		44	26		107				
F37	$1866 - i\frac{255}{2}$	33	-5		-21			41	144
		26	29		4			-31 (Junk)	
		42	29		22			51	

Argand diagrams for the first time. We hope to resolve these solutions as soon as the amplitudes in the middle of the Saclay gap become available.

5.2 Monte Carlo tests and sensitivity limits

Before unleashing this big program on data, we tested it on Monte Carlo events. This is a fine way to debug the program. It also forecasts :-

- a. The number of events that will be needed for a unique fit.
- b. The sensitivity of the analysis - at what $|T|$ will we fail to find a Monte Carlo wave ?

Fig. 3 shows the very satisfying result of one of these Monte Carlo tests. Larry Miller played God (or Prince Rainier). As such he :-

a) Invented a secret list of eleven amplitudes (the dots of Fig. 3). Even the length (11) of the list was kept secret.

b) Generated a Monte Carlo "experiment" of 7500 events at 1690 MeV, corresponding to the 11 dots, and gave the "data summary tape" to another student, David Herndon.

Herndon started with all 60 possible waves, and came up with the 11 crosses on Fig. 3, plus 13 more "noise" waves, as big as the four smallest secret waves, but all inside the box shown on the figure, whose half-side is ± 0.05 . We conclude that our signal : noise is better than 1:1 only for $|T| > 0.05$.

Given the extra uncertainties and systematic errors of real data (where our model can also not be perfect), we prefer to quote a "sensitivity" of $|T| \sim 0.1$.

The same experiment fails when tried with only 2500 instead of 7500 events (we find many solutions); and works poorly with 5000 events (several solutions). Hence our slogan that we need $\sim 10,000$ events at each energy in the region of 1690 where we have to consider 60 waves.

5.3 Sign checks

Our programs can be internally consistent, pass the Monte Carlo tests of Section 5.2, and still have a wrong sign or sign convention, e.g. for a Clebsch-Gordan coefficient or a D-function. So we decided to put the same data through all the programs available, from Oxford^{8,9)}, Saclay¹⁰⁾ and LBL/SLAC. None of the results agreed in all waves! We found a bug or a misunderstanding in both our own program and our version of Saclay's old program; Oxford won. Now that independent programs agree, we tend to believe them.

Table II-4.

Comparison of resonance parameters from (a) coupling estimate and elastic phase shift analysis; (b) poles of the T-matrix; and (c) unitary (Breit-Wigner + background) fit.

	M	Γ_{tot}	πN	$\pi \Delta$	$\pi \Delta$	$N\rho$	$N\epsilon$	
D15	1670	141	56	75				Elastic/coupling estimate ^a
	1666	159	69	92				T-matrix pole ^b
	1692	176	71	105				Unitary (BW + background) ^c
F15	1690	133	80	21		16	13	Elastic/coupling estimate ^a
	1672	155	101	12		42	21	T-matrix pole ^b
	1682	153	88	15		33	17	Unitary (BW + background) ^c
F35	1890	260	40	16		140		Elastic/coupling estimate ^a
	1824	282	44	26		107		T-matrix pole ^b
	1907	324	51	55		219		Unitary (BW + background) ^c
D13	1520	119	68	15	9	20		Elastic/coupling estimate ^a
	1514	142	89	36	14	34		T-matrix pole ^b
P13	1850	250	63			195		Elastic/coupling estimate ^a
	1728	159	25			84		T-matrix pole ^b

- a) using results from elastic analyses⁴⁾ (Breit-Wigner and background fit to elastic Argand diagram) together with "eye-ball" estimates of coupling from Argand diagram;
- b) T-matrix pole quantities from the K-matrix parametrization;
- c) unitary (Breit-Wigner plus background) refit to smooth Argand diagrams from K-matrix parameters.

The implication of these statements is that it is not easy (and sometimes impossible) to relate pole parameters to the parameters of the Breit-Wigner amplitude which we normally discuss. This point will be demonstrated more in the following sections.

It does appear, however, that these pole parameters are unique (if calculated in the same manner with equally good fit to data), and thus it will be necessary for any future theories to present the results on resonances in terms of the properties of the corresponding second sheet poles (or whichever sheet is appropriate in the specific multi-channel problem).

6. UNITARY (BREIT-WIGNER AND BACKGROUND) FITS TO THE T-MATRIX

In order to better estimate the conventional Breit-Wigner parameters, we assume that in the region of a pole our T-matrix amplitude can be described as a Breit-Wigner plus unitary background:

$$T(\text{refit}) = T^{\text{BW}} + T^{\text{Bkgd}}, \quad (10)$$

where

$$T_{ij}^{\text{BW}} = \frac{\frac{1}{2} \Gamma_i \Gamma_j}{E_R - E - \frac{i}{2} \sum_k Y_k^2 Q_k}, \quad (11)$$

$$\Gamma_j = Q_j^{\frac{1}{2}} \gamma_j e^{i\theta_j}, \quad (12)$$

and the background S-matrix ($S = 1 + 2iT$) is separately unitary,

$$S_{ij}^{\text{Bkgd}} = \delta_{ij} + 2i Q_i^{\frac{1}{2}} T_{ij}^{\text{Bkgd}} Q_j. \quad (13)$$

As in Eqs. (3) and (4), T^{Bkgd} is parameterized as a K-matrix (this time a linear function of E) and the BW phase θ_j is adjusted by a matrix unitarity constraint¹⁵⁾

$$S^{\text{Bkgd}} \Gamma^* = \Gamma. \quad (14)$$

Unfortunately a general multichannel solution of Eq. (14) is not possible, so we added Eq. (14) as an additional chi-square term and fitted θ_j as a polynomial in E ¹²⁾.

One can see that as the number of channels increases the number of parameters rises sharply. Because of this limitation, these fits are time-consuming.

Once the parameters of the B.W. refit are found, we can recalculate $T(\text{refit})$ via Eq.(10) and again hunt for its poles. We find that this (indirect) pole is close to that of the original amplitude, if (and only if) we have imposed the unitarity constraint (14). This agreement must mean that, near a resonance, Eq. (10) is a good approximation. Thus we have found a self-consistent way to parameterize a resonance, but we repeat our earlier warnings about the differences between pole parameters and BW parameters, both of which are plotted in Table 4:

1) The 2 sets of parameters do not (and cannot) always agree.

2) The BW parameters depend on the form chosen for the background, while of course the parameters of the pole itself should be stable against changes in the form of the background.

7. RESULTS FROM THE DIFFERENT RESONANCE PARAMETERISATIONS

In Table 4 we have compared the various parameters obtained for the resonances by the several methods discussed above:

We think the lessons of this table are clear:

- i) for clear narrow resonances, e. g., D13, F15, D15, one obtains reasonable qualitative agreement although quantitatively there are factors of 2 (or more) disagreement in partial widths;
- ii) for wide resonances, e. g., P13, F35, the displacement of M (conventional) and $\text{Re}l(E_{\text{pole}})$ can be on the order of 100 MeV.

The above observations mean that one should be wary of using quoted resonance parameters without checking their origin and, further, the partial widths are only reliable to factors of ~ 2 .

8. CONCLUSIONS

- 1) We have measured 23 couplings in sign and magnitude and this will be an important testing ground for any new theories.
- 2) It is possible to obtain good representation of the Argand diagrams in all channels and then extract the pole structure of the T matrix. This has been done for all the resonances we observe with $E < 2000$ MeV.
- 3) It is not possible in general to relate the pole parameters unambiguously to the parameters of Breit-Wigner. In order to obtain such quantities it is necessary to make a fit to the data with a unitary model resonance plus background. We have obtained such for three pronounced resonances.
- 4) The uniqueness of the pole parameters indicated in analyses of elastic P33 amplitude seems to be present in the inelastic waves we have considered.
- 5) The various theoretical calculations are consistent with our results only for our 1973 continuation across the energy gap. It is clearly essential to obtain partial wave amplitudes in this region as soon as possible.

9. ACKNOWLEDGEMENTS.

I want to thank Frixos Triantis for carefully reading these lectures and suggesting improvements. I am grateful to DPhPE at Saclay, and particularly to Mme. M. Thellier, for typing this manuscript.

REFERENCES FOR LECTURE II.

- 1) R.G. Moorhouse and H. Oberlack, Phys. Letters 43B, 44 (1973);
R.G. Moorhouse, H. Oberlack and A.H. Rosenfeld, LBL-1590 (submitted to
Phys. Rev. (July 1973)).
- 2) R.G. Moorhouse and N. Parsons, Comparison of the Quark Model with SU(3)
Inelastic Amplitudes University of Glasgow, G128QQ. (submitted to
Nucl. Phys. B. (July 1973)).
- 3) CERN-Heidelberg-Saclay Collaboration, J. Prevost et al.
DPhPE 73-07, June 1973.
- 4) H. Melosh IV, California Institute of Technology preprint, June 1972
(unpublished).
- 5) D. Faiman and J. Rosner, Ref. TH-1636 CERN (1973).
- 6) F. Gilman, M. Kugler, and S. Meshkov, SLAC Report SLAC-PUB-1235 (1973).
- 7) R. Ayed, P. Bareyre, Y. Lemoigne, contributed paper to the XVI Interna-
tional Conference on High Energy Physics, Batavia, Illinois (1972).
- 8) S. Almeded and C. Lovelace, Nucl. Phys. B40, 157 (1972).
- 9) Particle Data Group, Phys. Letters 39B, 1 (1972).
- 10) H. Pilkuhn, The Interactions of Hadrons (John Wiley, New York 1967), Ch. 8.
- 11) J. M. Blatt and V. F. Weisskopf, Theoretical Nuclear Physics (John Wiley, New
York, 1952).
- 12) R. S. Longacre (Ph. D. thesis), Lawrence Laboratory Report LBL-948 (1973),
unpublished.
- 13) T. A. Lasinski and A. Barbaro-Galtieri, Phys. Letters 39B, 1 (1972).
- 14) J. S. Ball, R. R. Campbell, P. S. Lee, and J. L. Shaw, Phys. Rev. Letters 28,
1143 (1972).
- 15) C. J. Goebel and K. W. McVoy, Phys. Rev. 164, 1932 (1967).

LEGAL NOTICE

This report was prepared as an account of work sponsored by the United States Government. Neither the United States nor the United States Atomic Energy Commission, nor any of their employees, nor any of their contractors, subcontractors, or their employees, makes any warranty, express or implied, or assumes any legal liability or responsibility for the accuracy, completeness or usefulness of any information, apparatus, product or process disclosed, or represents that its use would not infringe privately owned rights.

TECHNICAL INFORMATION DIVISION
LAWRENCE BERKELEY LABORATORY
UNIVERSITY OF CALIFORNIA
BERKELEY, CALIFORNIA 94720